

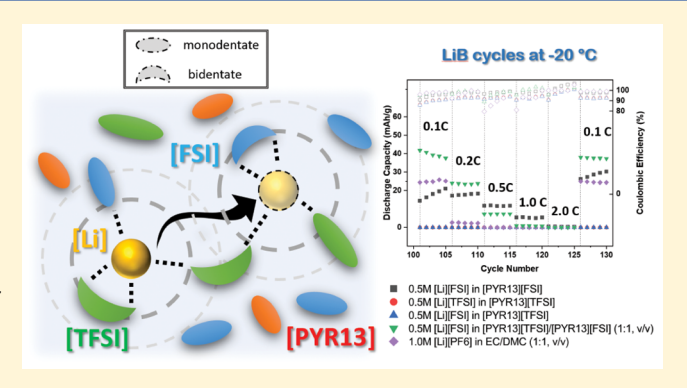
# Pyrrolidinium Ionic Liquid Electrolyte with Bis(trifluoromethylsulfonyl)imide and Bis(fluorosulfonyl)imide Anions: Lithium Solvation and Mobility, and Performance in Lithium Metal-Lithium Iron Phosphate Batteries

Qianwen Huang, Yun-Yang Lee, and Burcu Gurkan\*

Department of Chemical and Biomolecular Engineering, Case Western Reserve University, Cleveland, Ohio 44106, United States

Supporting Information

**ABSTRACT:** A mixture of *n*-methyl-*n*-propylpyrrolidinium bis(trifluoromethylsulfonyl)imide, [PYR13][TFSI] and npropyl-n-methylpyrrolidinium bis(fluorosulfonyl)imide, [PYR13][FSI] ionic liquids (ILs) is investigated for lithium-metal batteries. Specifically, the relation among conductivity, solvation structure, and Li+ mobility is investigated in a Li/IL/IL type ternary mixture. Li<sup>+</sup> anion coordination numbers with both [TFSI] and [FSI] in the ternary mixtures are derived from Raman analysis. The Li+ transference number was measured by a combination of potentiostatic polarization and electrochemical impedance spectroscopy (EIS) techniques. The electrochemical stability and transport property of the developed ternary mixture were



confirmed with Li-Li symmetrical and Li-LiFePO<sub>4</sub> cells. The ternary system exhibited improved rate capability compared to binary parent electrolytes as well as the state-of-the art carbonate-based electrolyte at -20 °C, and slightly better cycling stability at 25 °C. This study demonstrates the flexibility in tailoring physical properties and the Li<sup>+</sup> solvation environment by ternary Li/ IL/IL mixtures for enhanced battery performance.

#### ■ INTRODUCTION

Ionic liquid (IL) electrolytes present favorable properties such as high thermal stability, wide electrochemical windows, negligible vapor pressures, and lack of flammability for electrochemical processes. In particular, pyrrolidinium-based ILs with bis(trifluoromethylsulfonyl)imide, [TFSI], and bis-(fluorosulfonyl)imide, [FSI], anions have been commonly investigated for lithium ion and lithium metal batteries due to their exceptionally high electrochemical stability (5–6 V vs Li/ Li<sup>+1,2</sup>). These ILs are reported to inhibit the dendrite formation on lithium metal and lithiated graphite by forming a stable solid-electrolyte interphase (SEI), thus offering longterm cyclability of rechargeable high energy-density batteries.<sup>3–8</sup> However, Li<sup>+</sup> mobility and therefore the rate performance of these batteries with ILs remains a challenge in practice due to the high viscosities and low conductivities of Li<sup>+</sup>-containing IL electrolytes<sup>9-11</sup>

The Li<sup>+</sup> transport properties in ILs are highly dependent on Li salt concentration and Li+ solvate structure. 12-16 Yoon et al. 17 demonstrated fast charge/discharge (0.1-5 C) of lithium metal batteries with n-propyl-n-methylpyrrolidinium bis-(fluorosulfonyl)imide, [PYR13][FSI], containing high lithium salt concentration (3.2 mol/kg of [Li][FSI], calculated to be about 4.48 M when assuming the density of the solution is 1.4 g/cm<sup>3</sup>). Despite the low conductivity and high viscosity of the studied electrolyte, Li<sup>+</sup> transference was observed to increase with higher concentrations of the Li-salt. Therefore, the authors concluded that the Li<sup>+</sup> transport mechanism must be different in these concentrated electrolytes compared to those with lower Li-salt content. Haskins et al. 18 performed a combined experimental and computational study on the Li+ containing imidazolium and pyrrolidinium ILs. They report the vehicular motion of  $Li^+$  ( $Li^+$  transport with its solvation shell) to be significant across all concentrations studied (0.1 <  $x_{\text{Li-salt}}$ < 0.33) and the transport via anion exchanges (structure diffusion) becomes significant at higher mole fractions of Lisalt specifically for ILs with larger anions such as [TFSI].

Several studies to date investigated the ion coordination and solvation of Li<sup>+</sup> in IL electrolytes to better understand the Li<sup>+</sup> transport mechanism. 14,19-28 The Raman studies  $^{12,1} \bar{\textbf{4}}, ^{19-25,27-33}$  to express Li $^{\scriptscriptstyle +}$  coordination number related primarily to the vehicular motion have almost exclusively considered binary electrolytes (a Li-salt in an IL) with the

Special Issue: Chuck Eckert Festschrift

Received: June 13, 2019 Revised: September 16, 2019 Accepted: October 3, 2019 Published: October 3, 2019

exception of our previous work<sup>15</sup> on [Li][TFSI]/[PYR13]-[TFSI]/[EMIM][DCA] ternary system. Lesch et al.<sup>34</sup> studied the Li<sup>+</sup> coordination and transport in ternary IL mixtures of [EMIM][FSI]/[EMIM][TFSI]/[Li][TFSI] via MD simulations and pulsed gradient NMR. Their research showed that Li<sup>+</sup> prefers to coordinate with [TFSI] and form dimers ([TFSI] bridging two nearby Li<sup>+</sup>) as the [TFSI] fraction increases in the mixture. Interestingly, the diffusivities of dimerized and single Li<sup>+</sup> (not part of a dimer) were similar despite the different solvation structures, possibility as a result of the roughly equivalent size of the Li<sup>+</sup>-dimers and [Li][TFSI] aggregates. They further concluded that the anion exchange rate did not influence Li+ transport for these electrolytes containing dimers and aggregates, in contradiction to their previous study<sup>35</sup> where Li<sup>+</sup>-anion exchanges in [Li][TFSI]/ [PYR14][TFSI] were found to slow Li<sup>+</sup> transport under biased potential.

Mixed electrolytes beyond binary systems stem from the need to fine-tune physical, electrochemical, and transport properties for battery applications. The concept of electrolyte formulation to take advantage of each component is not new, and it is commonly practiced for carbonate based electrolytes.<sup>36–39</sup> Recently, IL mixtures have also been reported as electrolytes for batteries. Appetecchi et al.40 reported the composition and temperature dependence of the electrochemical window and conductivity for [Li][PF6] and [Li]-[TFSI] containing a [PYR14][TFSI]/[PYR13][FSI] mixture for which an increase in [PYR13][FSI] in general led to improvements in conductivity. Lux et al.<sup>41</sup> investigated the ternary electrolyte, 0.3 M [Li][TFSI] in ([PYR13][FSI])<sub>0.25</sub>/ ([PYR14][TFSI])<sub>0.75</sub> with the addition of 5 wt % vinyl carbonate, in Li-graphite half cells and reported a specific capacity of 290 mAh/g at room temperature; significantly higher than the respective salt-IL binary systems with 5 wt % vinyl carbonate additive (both around 130 mAh/g). Bayley et al. 13 studied the transport properties of [PYR13][TFSI]/ [PYR13][FSI] binary and [Li][TFSI]/[PYR13][TFSI]/ [PYR13][FSI] ternary mixtures. The diffusion coefficient of Li+, [PYR13], [TFSI], and [FSI] all showed an increasing trend with the increase of [FSI] in the mixture. Moreno et al. 42 optimized the composition of the ternary electrolyte [Li]-[TFSI]/[PYR13][TFSI]/[PYR13][FSI] for maximum conductivity and performed preliminary battery tests for only seven cycles at 0.1 C-rate and 23 °C with Li-NMC (nickel manganese cobalt oxide) and Li-graphite cells. The NMC and graphite electrodes with Li/IL/IL ternary mixture delivered 80 and 67%, respectively, of their expected capacities with conventional carbonate electrolytes. Because of the promising results of these initial tests, further investigation is deserved of the ternary [TFSI]- and [FSI]-based IL electrolytes for safer Li-metal batteries.

In this study, we investigated Li<sup>+</sup> mobility by transference measurements and Li<sup>+</sup> coordination structure in the ternary [Li][FSI]/[PYR13][TFSI]/[PYR13][FSI] electrolyte by Raman spectroscopy. Thermal, electrochemical and physical properties of the formulated electrolytes are measured as a function of Li-salt and temperature. To understand how Li+ transference and solvation structure influenced the rate capability and long-term cyclability of rechargeable Libatteries, we performed battery tests with Li-Li symmetrical cells at 25 °C and Li-LiFePO4 cells at 0.1-2 C rates and at temperatures of -20 to 120 °C.

### METHODS

Materials. N-methyl-n-propylpyrrolidinium bis-(trifluoromethylsulfonyl)imide ([PYR13][TFSI], 99.5%) was purchased from Iolitec (Tuscaloosa, Alabama); n-propyl-nmethylpyrrolidinium bis(fluorosulfonyl)imide ([PYR13][FSI], 99.9%) was purchased from Solvionic (France). Lithium bis(fluorosulfonyl)imide ([Li][FSI], >98.0%) was purchased from TCI America: bis(trifluoromethane)sulfonimide lithium salt ([Li][TFSI], 99.95%) was purchased from Sigma-Aldrich; polyvinylidene difluoride (PVdF,  $M_w \sim 534$  kDa) and 1 M lithium hexafluorophosphate ([Li][PF<sub>6</sub>]) in ethylene carbonate (EC)/dimethyl carbonate (DMC) (1:1, v/v) were purchased from Sigma-Aldrich; N-methyl-2-pyrrolidone (NMP, >99%) was purchased from Alfa Aesar. All the ILs and Li salts were used as purchased. The mixture of [PYR13][TFSI]:[PYR13][FSI] was prepared with a volumetric ratio of 1:1. The Li salt was dissolved in the ILs in the concentration range of 0.1-1 M. LiFePO<sub>4</sub> (LFP) powder, conductive graphite powder (CG; >99.98%), SS316 CR2032 case, Al-clad CR2032 case, and precoated LFP electrode sheets with an active material coating density of 12 mg cm<sup>-2</sup> were purchased from MTI (Richmond, CA). Glass fiber nonwoven separator (Whatman grade GF/A, 260  $\mu m$  in thickness) was purchased from VWR. Solupor 3P07A polyethylene (PE) film (20  $\mu$ m in thickness) was gifted by Lydall Inc. All chemicals were used as received without further purification and were handled in an argon purged glovebox (VTI Super, <1 ppm moisture and oxygen).

**Physical Properties.** Temperature-dependent density, viscosity, and conductivities were measured. The water content of samples was measured in the ppm range with a Karl Fischer titrator (Metrohm Coulometric KF 889 D). The reported water contents in Table S1 represent the typical range of water in all of the studied samples prior to measurements. The samples were never exposed to air prior or during the physical property measurements. Densities in the temperature range of 25-55 °C (±0.02 °C) were measured with an Anton Paar vibrating U-tube density meter (DMA 4500M) with an accuracy of 0.00005 g/cm<sup>3</sup>. Viscosities were measured with a microchannel viscometer with a 10 to 20 µL sample (MicroVISC, Rheosense) at 25-55 °C (±0.15 °C). Within the same temperature range, conductivities were measured by electrochemical impedance spectroscopy (EIS) (BioLogic SP 240) using 500  $\mu$ L sample with a calibrated two-electrode conductivity cell equipped with parallel Pt electrodes (MCM-CC, Biologic). The Vogel-Fulcher-Tamman (VFT) model<sup>43–45</sup> was fitted to both viscosity and conductivity.

Thermal Properties. Phase transformations such as crystallization and melting were determined by differential scanning calorimetry (DSC, TA Q100). The samples (about 5 mg) were first cooled from 40 °C to -80 °C at 10 °C/min followed by an isotherm at -80 °C for 5 min, then heated to 100 °C at a constant rate of 10 °C/min followed by a final isotherm step at 100 °C for 5 min, similar to the previous procedure. 13 This procedure was repeated three times, and the third cycle is reported. The glass transition temperature was not observed due to the limitation of the instrument (>-80

Li<sup>+</sup> Transference. The Li<sup>+</sup> transference number was measured in Li-Li symmetric cells by the Bruce and Vincent 46 method of potentiostatic polarization. Briefly, 10 mV DC voltage was applied to the cell until a steady current was established (2 h). EIS measurement was performed before and after the polarization step, at open circuit potential between 10<sup>-2</sup> to 10<sup>6</sup> Hz with 5 mV amplitude voltage. The Li<sup>+</sup> transference number was calculated by eq 1:

$$t_{\text{Li}^{+}} = \frac{I_{s}R_{f}[\Delta V - I_{0}R_{1}^{0}]}{I_{0}R_{i}[\Delta V - I_{s}R_{1}^{s}]}$$
(1)

where  $R_i$  and  $R_f$  are the initial and final resistances of the electrolyte,  $R_1^0$  and  $R_1^s$  are the initial and final resistance of the interfacial layer of Li metal electrode/electrolyte,  $I_0$  and  $I_s$  are the initial and stable current during 2 h polarization, and  $\Delta V$  is the applied DC voltage.

Li-Li Symmetrical Cell Fabrication. Li-Li symmetrical cells were assembled in an argon filled glovebox (VTI Super, < 1 ppm moisture and oxygen). Li metal was carefully polished by a 1000-grit sandpaper and the metal surface was flat-rolled to be smooth prior to use. Symmetrical cells were assembled with either glass fiber or Solupor PE film separator and the ternary electrolyte of 0.5 M [Li][TFSI] in [PYR13][TFSI]/ [PYR13][FSI] (1:1, v/v) using SS316 CR2032 casings. An electronic crimper (MSK 160E, MTI) was used to seal and disassemble coin cells. Assembled cells were stored at 60 °C overnight before testing to encourage wetting of the electrodes by the electrolyte and initial passivation layer to form at electrode-electrolyte interfaces.

Li-LFP Cell Fabrication. The electrode slurry for fabricating the LFP electrodes was prepared by mixing the finely ground LFP and conductive graphite powder in a polymeric solution of 2.9 wt % PVdF in NMP under stirring (ca. 200 rpm) at least for 2 days. The obtained slurry of LFP:CG:PVdF (80:10:10) was cast onto aluminum foil with a wet membrane thickness of 10  $\mu$ m by a doctor blade. The wet film was then immediately transferred to a vacuum oven at 60 °C. After the film was dried in the oven for 1 h, it was allowed to cool down to room temperature. The dried sheet (5  $\mu$ m) was compressed between two mechanical rollers and cut into electrode disks by a 5/8 in. diameter puncher. The electrodes were vacuum-dried at 120 °C overnight before the coin cell assembly to remove any residual moisture. The average coating density of the fabricated LFP cathode electrodes is about 1.5 mg cm<sup>-2</sup>, which is the active material loading used in capacity calculations. Alternatively, precoated Al sheets with LFP (MTI Inc.; 12 mg cm<sup>-2</sup> mass loading) were used. Electrodes were punched out to 5/8 in. diameter. Electrode weight was performed with a semimicrobalance with an accuracy of 0.02 mg (Sartorius QUINTIX65-1S). Nonwoven glass fiber (3/4 in. diameter) was applied as the separator and wetted with the electrolyte (70 µL) before battery assembly in a vacuum oven at 70 °C. The cells were prepared by laminating a Li metal anode, a glass fiber separator, and an LFP electrode cathode within the 2-electrode CR2032 configuration. Coin cells with five different types of electrolyte were fabricated: 0.5 M [Li][FSI] in [PYR13][FSI], 0.5 M [Li][TFSI] in [PYR13]-[TFSI], 0.5 M [Li][FSI] in [PYR13][TFSI], 0.5 M [Li][FSI] in [PYR13][TFSI]/[PYR13][FSI] (1:1, v/v), and 1 M [Li][PF<sub>6</sub>] in EC/DMC (1:1, v/v). LFP cells with high mass loading were fabricated with three types of electrolytes: 0.5 M [Li][FSI] in [PYR13][FSI], 0.5 M [Li][FSI] in [PYR13]-[TFSI]/[PYR13][FSI] (1:1, v/v), and 1 M [Li][PF<sub>6</sub>] in EC/ DMC (1:1, v/v). All cells were kept under 60 °C overnight before battery testing to allow the electrodes to be fully wetted

by the electrolyte and the initial passivation layer to form at the interface.

Battery Tests. Li-Li symmetrical cells with either glass fiber or Solupor PE separators were charged and discharged at 1 mA/cm<sup>2</sup> for 500 cycles and 10 mA/cm<sup>2</sup> for 100 cycles, sequentially. Each cycle took 60 min. EIS was performed before and after 500 cycles at 1 mA/cm<sup>2</sup> to characterize the change in cell impedance.

Li-LFP cells with 1.5 mg cm<sup>-2</sup> mass loading were cycled between 2.8-3.8 V at 0.1, 0.2, 0.5, 1.0, and 2.0 C with constant current (CC) at 25 and 60 °C for five cycles at each C-rate. The temperature was controlled within +0.5 °C using Espec BTZ-133 temperature chamber. For longer-term battery performance and thermal stability evaluation, the Li-LFP cells were first cycled at 25 °C for 100 cycles at 0.2 C then cycled for 20 at each temperature sequence of 60, 80, 100, and 120 °C. In parallel, a different set of Li-LFP cells were tested following a three-step cycling. The first step involved cycling at 0.2 C for 20 cycles following a temperature sequence of 25, 0, -10, -20 °C, and back to 25 °C. The second step was a ratecapability test for which the same set of cells were cycled at -20 °C at 0.1, 0.2, 0.5, 1, 2 and back at 0.1 C rates with five cycles at each C-rate. Finally, the third step was a long-term cycling stability test for which the same cells were cycled at 0.2 C-rate for 100 cycles at 25 °C.

Four Li-LFP cells with 12 mg cm<sup>-2</sup> mass loading were precycled at 0.1 C for three cycles at 25 °C prior to the ratecapability test at -20 °C and 0.1, 0.2, 0.5, 1.0, and back at 0.1 C with five cycles at each C-rate. EIS was performed before and after cycling at both temperatures.

Raman spectroscopy. The Li<sup>+</sup> coordination in the electrolyte systems was investigated by Raman spectroscopy (Xplore Horiba, 785 nm, 9 mW). The spectra was collected in the region of  $670-800 \text{ cm}^{-1}$  with a resolution of  $4.2 \text{ cm}^{-1}$  to observe the (-S-N-S-) stretching signal in [FSI] and [TFSI] anions that coordinate with Li<sup>+</sup>. The baseline correction was performed with NGS LabSpec software (Horiba). The peak fitting was performed with Igor Pro 7.08 (WaveMetrics) for which the residual of all the fittings were lower than 2% (corresponding to a  $\chi^2/I$  < 112, where *I* is the maximum Raman intensity recorded). The spectrum reported in the figures were normalized based on the maximum intensity. The Li<sup>+</sup> coordination numbers (CN) in the Li/IL/ IL ternary mixtures are reported according to eq 2.

$$CN = CN_{[FSI]} + CN_{[TFSI]}$$

$$= \frac{\frac{n_{[FSI]}}{n_{[FSI]} + n_{[TFSI]}} \cdot \frac{A_{III}}{A_{1} + A_{III}}}{x_{[Li][FSI]}} + \frac{\frac{n_{[TFSI]}}{n_{[TFSI]} + n_{[FSI]}} \cdot \frac{A_{IV}}{A_{II} + A_{IV}}}{x_{[Li][FSI]}}$$
(2)

in which  $\text{CN}_{\text{[FSI]}}$  and  $\text{CN}_{\text{[TFSI]}}$  correspond to the partial coordination number of Li+-[FSI] and Li+-[TFSI], respectively;  $n_{[i]}$  is the mole of ion i;  $A_i$  is the area of peak i; and  $x_{[LiESI]}$  is the mole fraction of [Li][FSI].

#### RESULTS AND DISCUSSIONS

The DSC curves shown in Figure 1 compare the [PYR13]-[TFSI]/[PYR13][FSI] (1:1, v/v) binary system to the two parent ILs. The IL/IL binary mixture has a lower melting point  $(-28.2~^{\circ}\text{C})$  compared to the parent ILs  $(8.4~^{\circ}\text{C})$  for [PYR13][TFSI] and -19.8/-11.3 °C for [PYR13][FSI]); these results are similar to the previous reports. 13,47,48 The measured temperature-dependent densities, viscosities, and

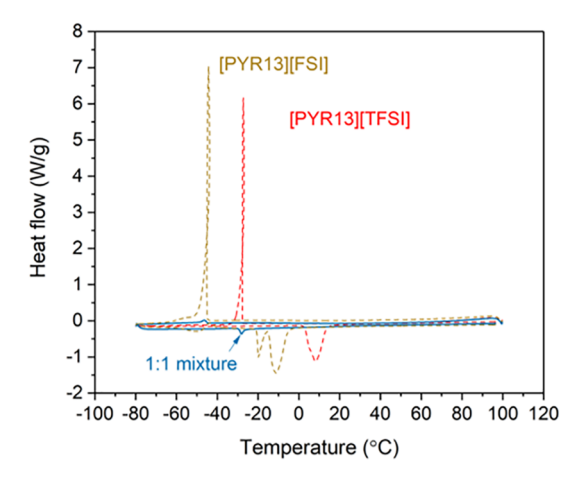


Figure 1. DSC curve of [PYR13][TFSI], [PYR13][FSI], and [PYR13][TFSI]/[PYR13][FSI] (1:1, v/v).

conductivities of the binary IL/IL, [Li][FSI]/IL, and ternary [Li][FSI]/IL/IL systems are in Figures S1-S3. The VFT fitting parameters of the viscosity and conductivity are shown in Table S2. These fittings enable extrapolation of the viscosities and conductivities of the IL-electrolytes at the cell-test temperatures as they relate to rate capabilities. Viscosity and conductivity measurements were used for the Walden analysis of IL/IL binary in comparison to neat ILs shown in Figure 2a and the 0.5 M [Li][FSI]/IL/IL ternary in comparison to [Li][FSI]/IL binaries shown in Figure 2b. According to the Walden plot in Figure 2a, the 1:1 IL/IL mixture shows a higher degree of ion association compared to neat ILs. Similarly, the [Li][FSI]/IL/IL ternary with 0.5 M [Li][FSI] in 1:1 demonstrates increased ion association compared to binary mixtures of [Li][FSI]/IL with the same Li-salt concentration, as seen in Figure 2b. Increased ion associations could be interpreted to result in ion aggregates which would impede vehicular motion of Li<sup>+</sup>. Solely based on this Walden analysis, it is difficult to make any conclusions about the extent of ion aggregates or Li<sup>+</sup> mobility. To better understand the first solvation shell of Li+ in these systems, Raman analysis is carried out.

Figure 3 shows the local Raman spectrum (670-800 cm<sup>-1</sup>) corresponding to the -S-N-S- stretch of [TFSI] and [FSI] anions in the ternary mixture of [Li][FSI] in [PYR13][TFSI]/ [PYR13][FSI] (1:1, v/v). The full Raman spectra (500-2000 cm<sup>-1</sup>) are shown in Figure S4. A broad peak centered at 754 cm<sup>-1</sup> is present at all concentrations of [Li][FSI] (0-1 M), and it is attributed to the [PYR13] cation. 33,49 In the absence of Li-salt, there are two distinct peaks at 727 and 741 cm<sup>-1</sup> that correspond to [FSI] and [TFSI] anions, respectively. With the addition of Li-salt, two new peaks emerge at 744 and 748 cm<sup>-1</sup> that correspond to Li<sup>+</sup> coordinated [FSI] and [TFSI] anions, respectively. As the concentration of Li-salt increases from 0 to 1 M in the mixture, the intensity and areal fraction of Li+ coordinated peaks grow as seen in Figure 3. This behavior is similar to the [Li][FSI]/[PYR13][FSI] (Figure S5) and [Li][TFSI]/[PYR13][TFSI]<sup>15</sup> binary systems. As more anions get coordinated with Li+, more ion clusters may form.

The calculated coordination number of Li<sup>+</sup> from eq 2 as a function of Li-salt concentration is presented in Figure 4. The partial solvation of Li<sup>+</sup> by [TFSI] and [FSI] anions in the ternary mixture are represented as CN<sub>TESI</sub> and CN<sub>ESI</sub> in Figure 4a. Accordingly, CN of both Li<sup>+</sup>-[TFSI] and Li<sup>+</sup>-[FSI] decreases with the increase of [Li][FSI] concentration, since both [TFSI] and [FSI] can have both monodentate and bidentate coordination conformation with Li+, which may lead to anion bridges among multiple Li<sup>+</sup>. When the coordination of Li<sup>+</sup> in the ternary mixture is compared with the respective binaries in Figure 4b, it is seen that the CN of Li<sup>+</sup> is highest when there is only [FSI]. This is due to the smaller size of [FSI] compared to that of [TFSI].<sup>50</sup> Therefore, we expect that the Li<sup>+</sup> would prefer to coordinate with [FSI] over [TFSI] in the ternary mixtures. However, according to Figure 4a, Li<sup>+</sup> prefers to coordinate with [TFSI] over [FSI] in the ternary mixture. This experimental observation agrees with the former finding of Lesch et al.<sup>34</sup> on a similar ternary system containing the [EMIM] cation. The Li<sup>+</sup> coordination in the ternary mixture is very similar to the [Li][FSI]/[PYR13][FSI] binary. This is interesting considering the higher ionicity observed for [Li][FSI] in [PYR13][FSI] compared to [PYR13][TFSI] or the ternary mixture of interest from the Walden analysis in Figure 2b. This observation underscores the complexity of

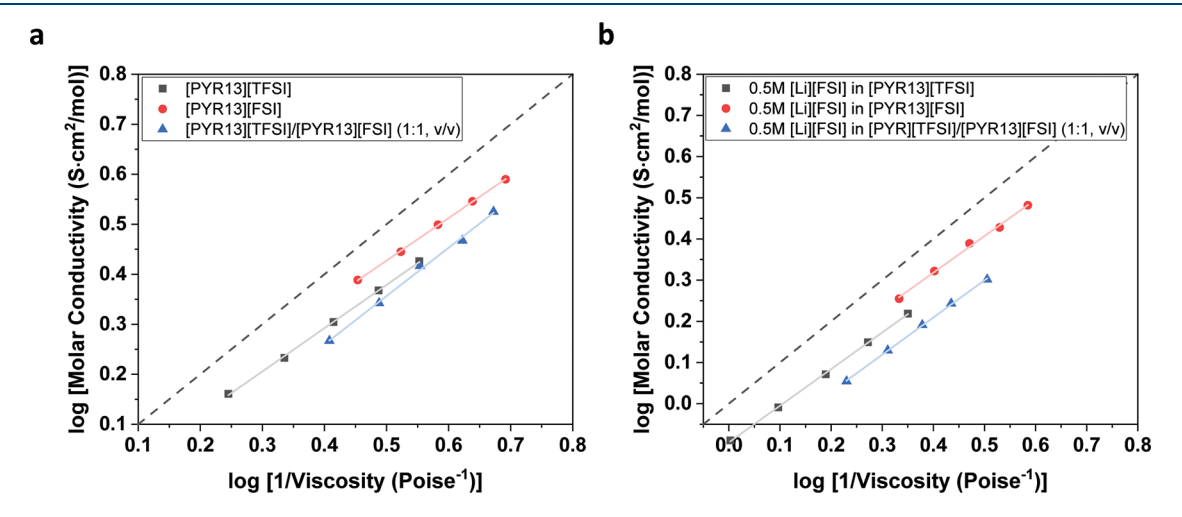


Figure 2. Walden plot of (a) [PYR13][TFSI]/[PYR13][FSI] binary mixtures compared with their parent ILs, and (b) 0.5 M [Li][FSI] in [PYR13][TFSI], [PYR13][FSI], and [PYR13][TFSI]/[PYR13][FSI] (1:1, v/v). The dashed line indicates the "ideal" electrolyte that is dissociated (0.01 M KCl<sub>(aq)</sub>), and the solid lines are linear fits to the measured data.

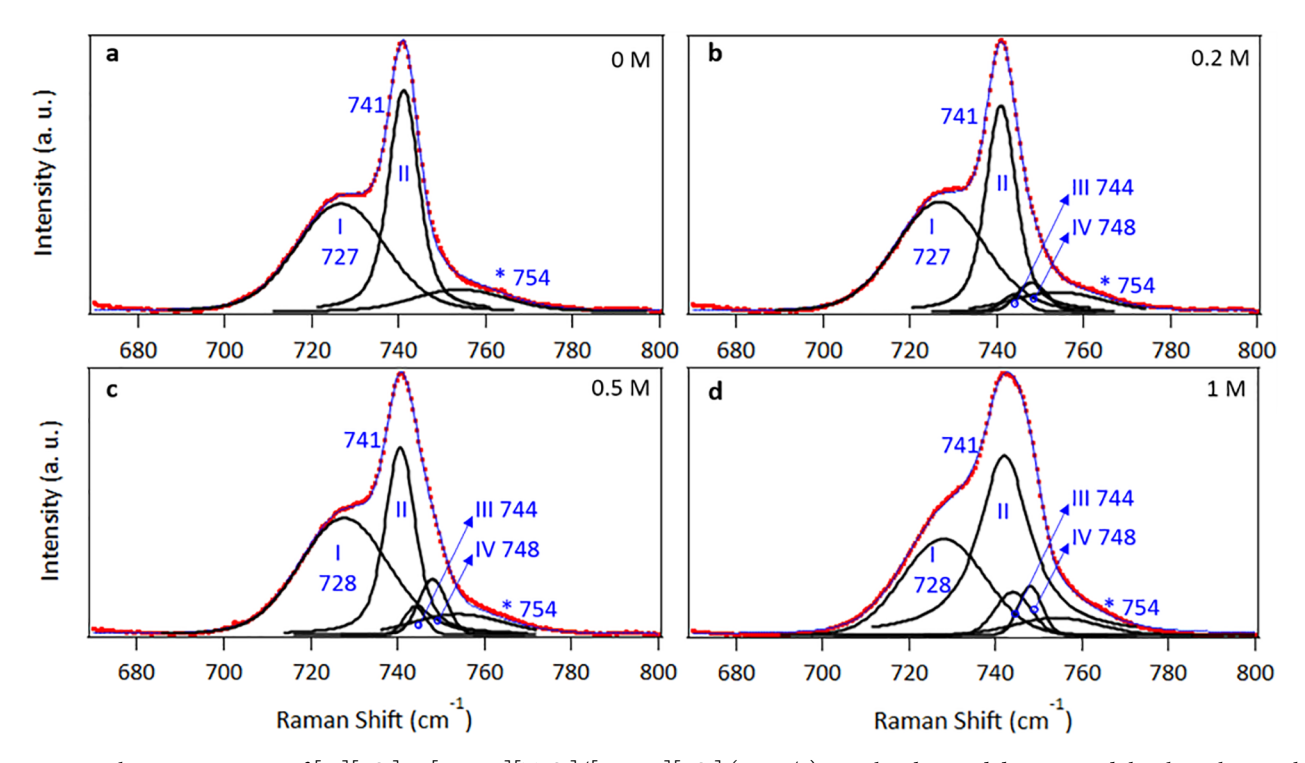


Figure 3. Local Raman spectrum of [Li][FSI] in [PYR13][TFSI]/[PYR13][FSI] (1:1, v/v). Panels a, b, c, and d correspond the electrolytes with 0, 0.2, 0.5, and 1 M [Li][FSI], respectively. Red symbols represent the collected data; black lines are the fitted Voigt peaks. Peaks labeled as I and II correspond to "free" [FSI] and [TFSI] vibrations, respectively. Peaks III and IV correspond to Li<sup>+</sup> coordinated [FSI] and [TFSI], respectively. The peak labeled with the asterisk (\*) appears in all systems, and it is attributed to [PYR13].

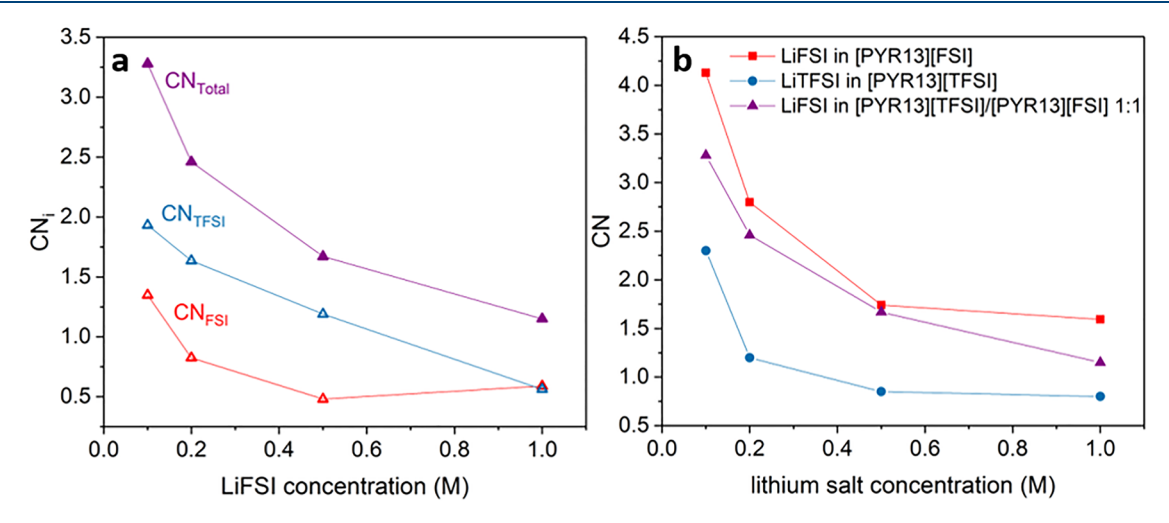


Figure 4. (a) Partial Li<sup>+</sup> coordination number in the [Li][FSI]/[PYR13][TFSI]/[PYR13][FSI] (1:1, v/v) ternary mixture and (b) total CN in [Li][FSI]/[PYR13][FSI] (red square), [Li][TFSI]/[PYR13][TFSI] (blue circle from ref 15), and [Li][FSI] in [PYR13][TFSI]/[PYR13][FSI] (1:1, v/v) ternary mixture (purple triangle).

clustering in these mixtures in comparison to the  ${\rm Li}^+$  coordination shell alone.

To probe how Li<sup>+</sup> solvation in these electrolytes impacts its mobility in an electric field, Li<sup>+</sup> transference was measured by the potentiostatic polarization method. Table 1 summarizes the measured and normalized transference numbers. Representative EIS and time-dependent DC polarization measurements for the ternary system are shown in Figure S6. The Li<sup>+</sup> transference increases slightly in the ternary mixture compared to the binary systems, suggesting that more Li<sup>+</sup> ions serve as charge carriers in the ternary mixture than in binary systems. However, one should note that 0.5 M concentration of Li salt

Table 1. Measured Li<sup>+</sup> Transference,  $t_{\text{Li}^+}$ , for the Binary and Ternary Electrolytes Studied. Transference Number Is Normalized by Li<sup>+</sup> Mole Fraction,  $t_{\text{Li}^+}/x_{\text{Li}^+}$ , for Relative Scale

molar composition	mole fractions	$t_{\mathrm{Li}^{^{+}}}$	$t_{\mathrm{Li}^{\scriptscriptstyle +}}/x_{\mathrm{Li}^{\scriptscriptstyle +}}$
0.5 M [Li][FSI] in [PYR13][FSI]	$\rm Li_{0.05}PYR13_{0.45}FSI_{0.5}$	0.15	3.00
0.5 M [Li][TFSI] in [PYR13][TFSI]	$\rm Li_{0.07}PYR13_{0.43}TFSI_{0.5}$	0.17	2.43
0.5 M [Li][FSI] in [PYR13][TFSI]/ [PYR13][FSI] (1:1, v/v)	$\rm Li_{0.06}PYR13_{0.44}TFSI_{0.20}FSI_{0.30}$	0.18	3.00

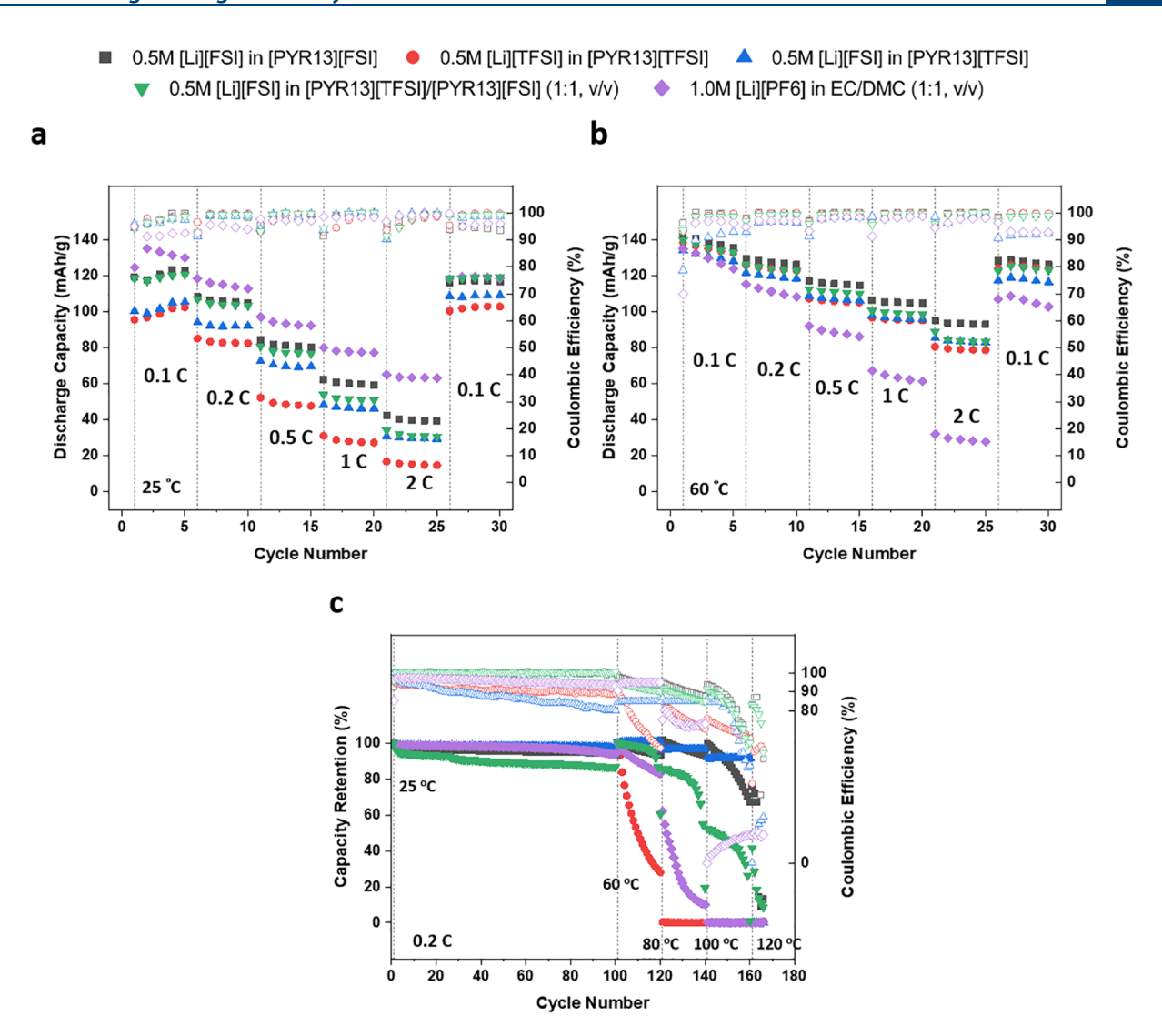


Figure 5. Li-LFP cell performance with 0.5 M [Li][FSI] in [PYR13][FSI], 0.5 M [Li][TFSI] in [PYR13][TFSI], and 0.5 M [Li][FSI] in [PYR13][TFSI]/[PYR13][FSI]/[PYR13][FSI] (1:1, v/v) mixtures. Specific discharge capacity (solid symbol) and Coulombic efficiency (open symbol) at 0.1–2 C-rates at 25 °C (a) and 60 °C (b). Long-term cycling at 25 °C followed by short cycling at 60, 80, 100, and 120 °C (c). Performances are compared with the state-of-the-art Li-ion battery electrolyte: 0.1 M [Li][PF<sub>6</sub>] in ethylene carbonate/dimethyl carbonate (EC/DMC, 1:1, v/v). Note that LIBs in panel b were constructed with Al-clad cell casing while those in panels a and c had SS316. Measurements shown in each panel a, b, and c were performed with fresh cells with 1.5 mg cm<sup>-2</sup> LFP electrode mass loading.

does not mean the same amount of Li+ is present in [PYR13][TFSI], [PYR13][FSI], and [PYR13][TFSI]/ [PYR13][FSI] (1:1, v/v). Therefore, the measured Li<sup>+</sup> transference number was normalized by the Li<sup>+</sup> mole fraction in each solution for a more direct comparison. According to this relative scale of  $t_{\text{Li}^+}/x_{\text{Li}^+}$ ,  $\text{Li}^+$  mobility in the ternary mixture is higher compared to [Li][TFSI]/[PYR13][TFSI] and similar to [Li][FSI]/[PYR13][FSI] binary. This result is not in agreement with the Walden analysis of ionicity, but similar to the trend in Li<sup>+</sup> coordination numbers which is related to the vehicular motion of Li<sup>+</sup>. On the other hand, the transference measurements are indicative of both Li+ diffusion with its solvation shell and migration. Anion exchanges within the ion clusters around Li<sup>+</sup> as a result of configurational changes can lead to jump motions of Li<sup>+</sup> which can explain the higher than expected transference in the ternary mixture despite the ion aggregates suggested by the Walden analysis.

Cycling with Li-Li symmetrical cells was performed to investigate the Li<sup>+</sup> transport and cathodic stability of the ternary IL system as a preliminary test for Li-LFP battery tests. The cells were cycled at constant current density of 1 and 10 mA/cm<sup>2</sup>. The voltage response in Figure S7 reveals the overpotential is initially high but stabilized to be within 20 mV at 1 mA/cm<sup>2</sup> and 150 mV at 10 mA/cm<sup>2</sup>. The characteristic sawtooth-like sinusoidal voltage profile indicates that the stripping and plating of the Li metal is stable and shows no evidence of Li dendrite formation, with a high Coulombic efficiency of >99.6% and >95.1% in cells with glass fiber and Solupor separator, respectively. Furthermore, the cells are capable of cycling under high current density; this behavior infers a practical Li+ transport property in the ternary IL electrolyte. It should be noted, however, that the cycling at 10 mA/cm<sup>2</sup> is possible only after precycling at low current density for SEI formation.

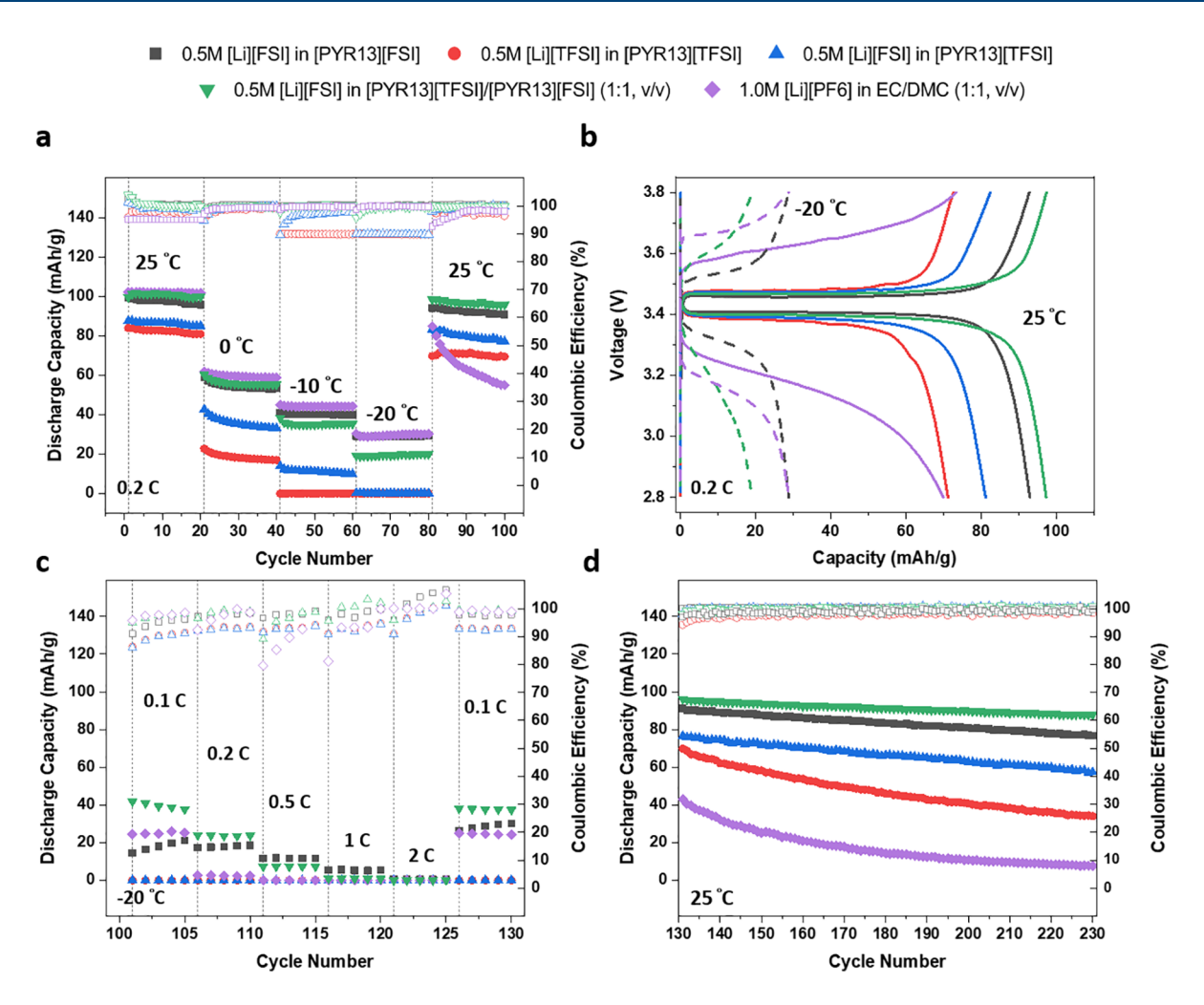


Figure 6. Prolonged cycling performance (solid symbols) and Coulombic efficiency (open symbols) of Li-LFP cells. (a) Discharge capacities at 25, 0, -10, -20 °C and back at 25 °C; (b) Charge—discharge curves at 25 °C (last segment in panel a) and -20 °C corresponding to the 20th cycle at both temperatures. (c) Rate capability tests at 0.1-2 C under -20 °C following the temperature-ramp test in panel a. (d) Long-term cycling at 25 °C and 0.2 C following the rate capability test in panel c. All of the IL-based electrolytes have 0.5 M Li-salt while the organic carbonate electrolyte has 1 M. All LIBs have Al-clad casing. Measurements in panels a, c, and d were all with the same set of cells (1.5 mg cm $^{-2}$  LFP electrode mass loading) following the testing sequence of panels a, c, and finally d.

Figure 5 panels a and b show the rate capability, on full depth of discharge (DOD), at 25 °C and 60 °C, respectively, for the Li-LFP coin cells with the binary and ternary IL-based electrolytes. For comparison purposes, the performance of the cell with the state-of-the-art carbonate electrolyte, 1 M [Li][PF<sub>6</sub>] in EC/DMC (1:1, v/v), is also presented. At 25 °C and 0.1 C, the ternary IL electrolyte cell exhibits a nominal specific capacity of around 120 mAh g<sup>-1</sup> (Figure 5a), similar with that of the least viscous [Li][FSI]/[PYR13][FSI] electrolyte cell. The measured capacity with the state-of-theart carbonate electrolyte is around 130 mAh g<sup>-1</sup> at 0.1 C and 25 °C, consistent with the expected theoretical capacity for LFP.<sup>51</sup> The capacity retentions after rate testing at 25 °C are 98.9, 94.9, and 91.2% for the ternary, [Li][FSI]/[PYR13][FSI] binary and the organic electrolyte, respectively, upon return to 0.1 C rate after five cycles at each C-rate from 0.1 to 2 C. As the rate increase from 0.1 to 2 C, the ternary IL cell performs similarly with [Li][FSI]/[PYR13][FSI]; both demonstrate about 13% capacity decay at 2 C compared to 0.1 C based on the fifth cycle. The traditional SS316 case was replaced by the Al-clad casing for rate capability tests at 60 °C (Figure 5b)

in order to eliminate the anodic dissolution effect when comparing the rate capabilities of the LIBs. The performance of all of the IL electrolytes at 60 °C exceed that of the commercial electrolyte cell at every C-rate studied (Figure 5b). An LIB with the ternary mixture exhibited a capacity retention of 92.5% upon return to 0.1 C at 60 °C (Figure 5b). While all of the IL-based electrolytes recovered >90% of their initial capacity, the carbonate-based electrolyte had only about 83%. At 60 °C (Figure 5b), the capacities are slightly higher for the cells with IL-based electrolytes compared to 25 °C due to the increased conductivity and reduced viscosity as predicted from VFT fits. This is not the case for the state-of-the-art carbonate electrolyte due to its thermal instability. Figure 5c shows the capacity retention upon 100 cycles at 25 °C followed by short cycling at 60, 80, 100, and 120 °C at 0.2 C. In this test, Li-LFP cells with the ternary Li/IL/IL electrolyte demonstrates a capacity retention of 86.4% while both the organic carbonate based electrolyte and [Li][FSI]/[PYR13][FSI] have about 94% retention after 100 cycles at 25  $^{\circ}$ C. All of the studied LIBs lost significant capacity with the increase of temperature following the 100 cycles at 25 °C except for 0.5 M [Li][FSI] in

- 0.5M [Li][FSI] in [PYR13][FSI]
- ▼ 0.5M [Li][FSI] in [PYR13][TFSI]/[PYR13][FSI] (1:1, v/v)
- 1.0M [Li][PF6] in EC/DMC (1:1, v/v)

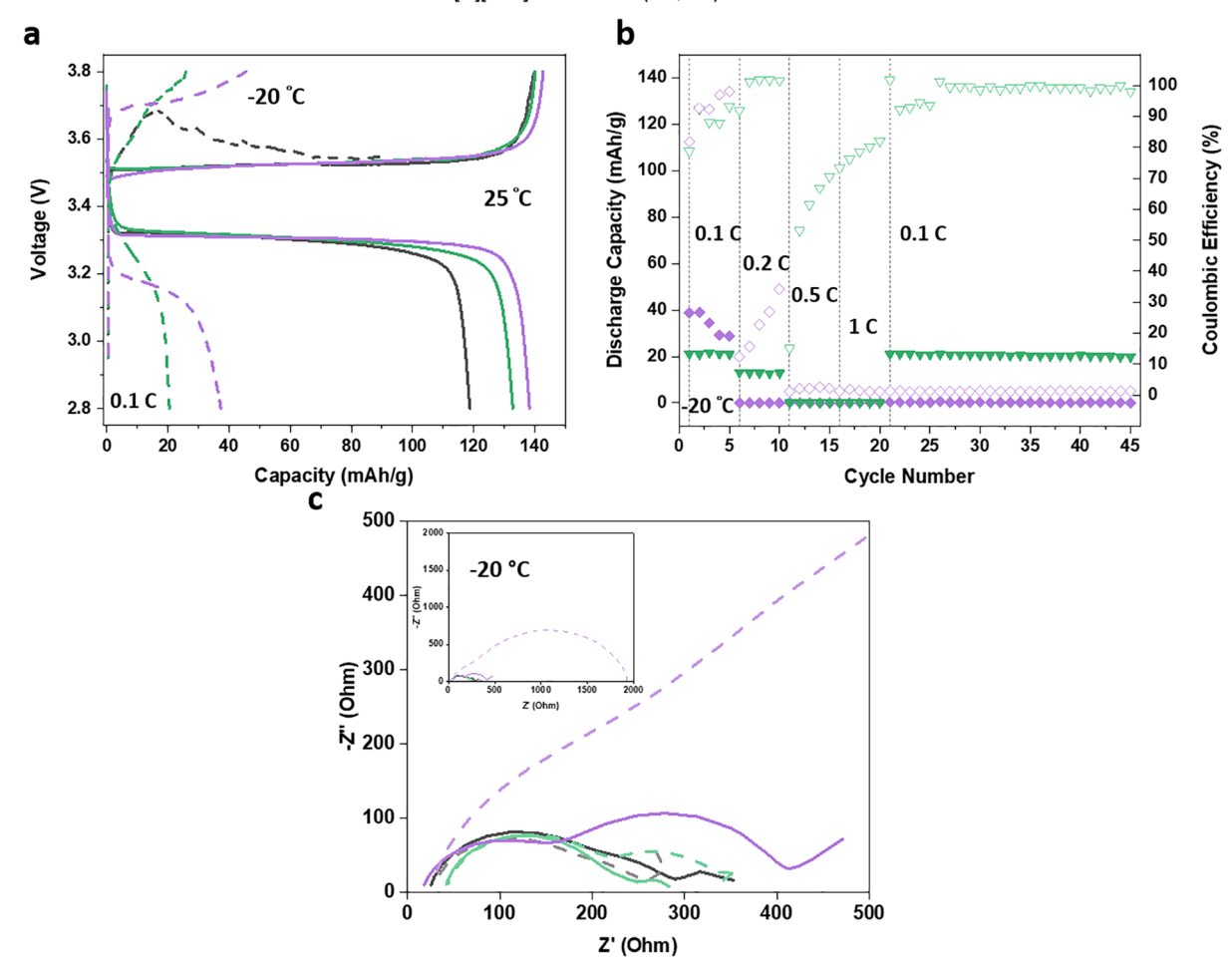


Figure 7. (a) Charge—discharge curves at 25 °C (3rd cycle at 0.1 C) and -20 °C (1st cycle at 0.1 C). (b) Rate capability tests at 0.1—1 C and -20 °C: cycling performance (solid symbol) and Coulombic efficiency (open symbol) of Li-LFP cells with 12 mg cm<sup>-2</sup> electrode mass loading. (c) EIS at -20 °C before (solid line) and after (dashed line) the rate cycling segment in panel b (0th and 25th cycles).

[PYR13][TFSI] which has 91.5% capacity retention by the fifth cycle at 100 °C compared to the first cycle at 25 °C. By 120 °C, all LIBs were exhausted. There are two main factors that govern the capacity trends in Figure 5c: (i) thermal stability and (ii) anodic metal dissolution from the SS316 cell case. 52,53 Swelling of the PVdF binder by the IL at high temperatures is also a possibility. On the basis of thermal analysis, [TFSI] leads to higher thermal stability<sup>54</sup> compared to [FSI]. However, LIB with 0.5 M [Li][TFSI] in [PYR13]-[TFSI] demonstrates a rapid decrease in capacity with increased temperature, in contrast to the expected higher thermal stability compared to other electrolytes studied. This capacity decay is hypothesized to be due to the enhanced Fe<sup>2+</sup> electrochemical dissolution from the metal cell case in the presence of [TFSI] and with increased temperature, more so then for [FSI]. This is in consideration of the extended cycling history of the LIBs with the SS316 cell casing in Figure 5c. The mixture of [TFSI]/[FSI] in the composition corresponding to the binary 0.5 M [Li][FSI] in [PYR13][TFSI] has an outcompeting capacity retention out of all the LIBs tested.

Due to a multitude of competing events at elevated temperatures, we lowered temperatures to distinctly study the impact of solvation on the rate capability. Figure 6a shows Li-LFP cells cycling at 25, 0, -10, -20 °C, sequentially and back to 25 °C at 0.2 C. At 25 and 0 °C, LIBs with ternary electrolyte exhibit similar battery capacity with [Li][FSI]/ [PYR13][FSI] binary and the organic electrolyte. At 25 °C, the ternary IL electrolyte cell exhibits a nominal specific capacity of around 100 mAh g<sup>-1</sup> (Figure 6a), which is in the same range of [Li][FSI]/[PYR13][FSI] and organic electrolyte cells. When the temperature is further decreased, all of the LIBs demonstrate decreased capacity due to decreased conductivity and increased viscosity. Upon return to 25 °C at the end of the temperature-ramp (from 25 to -20 °C), the capacity retention is the highest for the LIB with the ternary Li/IL/IL system at 96% while it was 94.7, 90.9, 85.8, and 54.2% for LIBs with [Li][FSI]/[PYR13][FSI], [Li][FSI]/[PYR13][TFSI], [Li]-[TFSI]/[PYR13][TFSI], and [Li][PF<sub>6</sub>]/EC/DMC, respectively (comparing the 20th cycle at 25 °C segments in Figure 6a). It is seen that the extent of the capacity decay with decreased temperature correlates with the [TFSI] content

among the IL-based electrolytes. Figure 6b shows the galvanostatic charge and discharge of the cells measured at  $^{\circ}$ C and  $^{\circ}$ C. It is observed that there is a longer plateau (associated with Li<sup>+</sup> deintercalation from LFP) in the voltage response with the IL-based electrolytes compared to the LIB with the organic carbonate electrolyte. Furthermore, this plateau is observed at lower potentials and with a less steep trend in the Li/IL and Li/IL/IL system, suggesting that there is higher resistance in the system with the organic electrolyte possibly due to the formation of a more resistive solidelectrolyte interface (SEI) layer at low temperatures. In the ILbased electrolytes, replacement of more [TFSI] with [FSI] seems to lead to a less resistive Li+ transport pathway across the SEI based on the voltage responses in Figure 6b. It should be noted that at -20 °C, neat [PYR13][TFSI] is a solid and [PYR13][FSI] is a semisolid, however the 1:1 mixture of [TFSI]/[FSI] with the [PYR13] common cation remains a liquid (Figure 1). Drawing parallels from this trend, it is anticipated that Li<sup>+</sup> mobility would be enhanced in the ternary Li/IL/IL at -20 °C, compared to the binaries studied. Figure 6c shows that the capacity retention after rate testing at -20°C is the highest for the Li/IL/IL ternary electrolyte with 99.2% (comparing the fifth cycles at the first and last 0.1 C segments). It should be noted that the cell with [Li][FSI]/ [PYR13][FSI] responds to rate testing at -20 °C unexpectedly, in particular at 0.1 C. However, it recovers in the followup long-term cycling test shown in Figure 6d. Finally, the ternary Li/IL/IL system demonstrates the highest capacity retention of all cells upon 100 cycles at 25 °C (Figure 6d) following low temperature histories in Figure 6a,c.

To study the impact of electrode mass loading on the rate capability, Li-LFP cells with higher cathode mass loading were tested at -20 °C. These cells were precycled for three cycles at 0.1 C and 25 °C, and it was confirmed that the nominal capacity of 140 mAh/g can be obtained as shown in Figure 7a. These cells were then subjected to charge-discharge cycles at 0.1, 0.2, 0.5, 1, and back at 0.1 C rate under −20 °C. Out of the three electrolytes tested in Figure 7a, only the cell with the ternary IL-electrolyte recovered capacity at the end of the rate capability test as seen in Figure 7b. The binary [Li][FSI]/ [PYR13][FSI] electrolyte is expected to be a semisolid at -20 °C with a significantly inhomogeneous and poor Li<sup>+</sup> transport as inferred from the conductivities and viscosities extrapolated by VFT, therefore even at 0.1 C it could not be charged to the target cutoff potential and was unable to deintercalate Li<sup>+</sup> from the cathode; leading to a waste of energy and no capacity. It is clearly seen that the cell capacity of [Li][PF<sub>6</sub>]/EC/DMC cell quickly decays, which might be mainly due to the significantly increased charge transfer resistance as seen in Figure 7c comparing the EIS before and after cycling at −20 °C. This is possibly due to the high resistive SEI layer that formed at low temperatures. Following the rate capability test, these cells were subjected to further cycling at 0.1 C, in which the cells with the ternary electrolyte maintains a capacity of about 20 mAh/g as seen in Figure 7b.

#### CONCLUSIONS

An IL-based ternary mixture of [Li][FSI]/[PYR13][TFSI]/ [PYR13][FSI] has been developed for potential applications as an electrolyte in Li-metal batteries and compared to its binary analogues in terms of physical properties and Li<sup>+</sup> transference. The ion coordination and interaction between Li<sup>+</sup> and anions were studied with Raman spectroscopy. The first solvation

shell of Li<sup>+</sup> in [PYR13]/[FSI] is similar to that in [PYR13]/ [TFSI]/[FSI] at the compositions studied in terms of the coordination numbers. While the Walden analysis suggests more ion aggregates beyond the first solvation shell in the ternary Li/IL/IL system compared to the Li/IL binaries, the rate capability and longer cycling of Li-LFP cells showed comparable performances in particular for [FSI]-containing mixtures at 25 °C. While it is proven challenging to decouple the impact of solvation and coordination number of Li<sup>+</sup> on rate capability from interferences such as SEI formation, anodic dissolution of the cell casing, and wettability of the electrodes at the coin cell level, it can be concluded that [Li][FSI]/ [PYR13][FSI] binary and [Li][FSI]/[PYR13][TFSI]/ [PYR13][FSI] ternary behave similarly at 25 °C, and the ternary system due to its utility of the eutectic IL mixture maybe more promising at subzero temperatures reaching to -20 °C. Both [Li][FSI]/[PYR13][FSI] binary and [Li][FSI]/ [PYR13][TFSI]/[PYR13][FSI] ternary showed excellent cycle reversibility and consistent capacity values, with higher than 99.5% Coulombic efficiency, even after hundreds of cycles under subzero temperatures. With increased electrode mass, the Li-LFP cells with the ternary IL-electrolyte was the only successful system with cyclable capacity at -20 °C, while the cells with the binary and the organic carbonate electrolytes fail due to poor Li<sup>+</sup> transport and high overpotential.

#### ASSOCIATED CONTENT

## S Supporting Information

The Supporting Information is available free of charge on the ACS Publications website at DOI: 10.1021/acs.iecr.9b03202.

Water content of samples, measured densities, viscosities and conductivites, VFT fit parameters, full Raman spectra, peak fits for an example binary Li/IL system, representative polarization and impedance data for transference measurements, voltage responses and EIS for Li–Li cell cycling (PDF)

#### AUTHOR INFORMATION

#### **Corresponding Author**

\*E-mail: beg23@case.edu.

#### ORCID (

Burcu Gurkan: 0000-0003-4886-3350

#### **Author Contributions**

<sup>†</sup>These authors contributed equally.

#### Notes

The authors declare no competing financial interest.

#### ACKNOWLEDGMENTS

This study was supported by NSF (CBET, Award No. 1903259).

# REFERENCES

(1) Li, Q.; Chen, J.; Fan, L.; Kong, X.; Lu, Y. Progress in Electrolytes for Rechargeable Li-Based Batteries and beyond. *Green Energy Environ.* **2016**, *1*, 18–42.

(2) Appetecchi, G. B.; Montanino, M.; Zane, D.; Carewska, M.; Alessandrini, F.; Passerini, S. Effect of the Alkyl Group on the Synthesis and the Electrochemical Properties of N-Alkyl-N-Methyl-Pyrrolidinium Bis(trifluoromethanesulfonyl)imide Ionic Liquids. *Electrochim. Acta* 2009, 54, 1325–1332.

- (3) Shkrob, I. A.; Marin, T. W.; Zhu, Y.; Abraham, D. P. Why Bis(fluorosulfonyl)imide Is A "Magic Anion" for Electrochemistry. *J. Phys. Chem. C* **2014**, *118*, 19661–19671.
- (4) Lewandowski, A.; Acznik, I. Impedance Study of Protecting Film Formation on Lithium and Lithiated Graphite Induced by Bis-(fluorosulfonyl) Imide Anion. *Electrochim. Acta* **2010**, *56*, 211–214.
- (5) Rothermel, S.; Meister, P.; Schmuelling, G.; Fromm, O.; Meyer, H. W.; Nowak, S.; Winter, M.; Placke, T. Dual-Graphite Cells Based on the Reversible Intercalation of Bis(trifluoromethanesulfonyl)imide Anions from an Ionic Liquid Electrolyte. *Energy Environ. Sci.* **2014**, *7*, 3412–3423.
- (6) Best, A. S.; Bhatt, A. I.; Hollenkamp, A. F. Ionic Liquids with the Bis(fluorosulfonyl)imide Anion: Electrochemical Properties and Applications in Battery Technology. *J. Electrochem. Soc.* **2010**, *157*, A903–A911.
- (7) Basile, A.; Bhatt, A. I.; O'Mullane, A. P. Stabilizing Lithium Metal Using Ionic Liquids for Long-Lived Batteries. *Nat. Commun.* **2016**, *7*, 1–11.
- (8) Howlett, P. C.; Macfarlane, D. R.; Hollenkamp, A. F. High Lithium Metal Cycling Efficiency in a Room-Temperature Ionic Liquid. *Electrochem. Solid-State Lett.* **2004**, *14*, 97–101.
- (9) Xu, K. Electrolytes and Interphases in Li-Ion Batteries and beyond. Chem. Rev. 2014, 114, 11503-11618.
- (10) Guerfi, A.; Duchesne, S.; Kobayashi, Y.; Vijh, A.; Zaghib, K. LiFePO<sub>4</sub> and Graphite Electrodes with Ionic Liquids Based on Bis(fluorosulfonyl)imide (FSI)- for Li-Ion Batteries. *J. Power Sources* **2008**, *175*, 866–873.
- (11) Elia, G. A.; Ulissi, U.; Jeong, S.; Passerini, S.; Hassoun, J. Exceptional Long-Life Performance of Lithium-Ion Batteries Using Ionic Liquid-Based Electrolytes. *Energy Environ. Sci.* **2016**, *9*, 3210–3220.
- (12) Zhou, Q.; Boyle, P. D.; Malpezzi, L.; Mele, A.; Shin, J. H.; Passerini, S.; Henderson, W. A. Phase Behavior of Ionic Liquid-LiX Mixtures: Pyrrolidinium Cations and TFSI- Anions Linking Structure to Transport Properties. *Chem. Mater.* **2011**, 23, 4331–4337.
- (13) Bayley, P. M.; Best, A. S.; MacFarlane, D. R.; Forsyth, M. Transport Properties and Phase Behaviour in Binary and Ternary Ionic Liquid Electrolyte Systems of Interest in Lithium Batteries. *ChemPhysChem* **2011**, *12*, 823–827.
- (14) Pitawala, J.; Kim, J.-K.; Jacobsson, P.; Koch, V.; Croce, F.; Matic, A. Phase Behaviour, Transport Properties, and Interactions in Li-Salt Doped Ionic Liquids. *Faraday Discuss.* **2012**, *154*, 71–80.
- (15) Huang, Q.; Lourenco, T. C.; Costa, L. T.; Zhang, Y.; Maginn, E.; Gurkan, B. Solvation Structure and Dynamics of Li<sup>+</sup> in Ternary Ionic Liquid Lithium Salt Electrolytes. *J. Phys. Chem. B* **2019**, *123*, 516–527.
- (16) Liu, H.; Maginn, E. Effect of Ion Structure on Conductivity in Lithium-Doped Ionic Liquid Electrolytes: A Molecular Dynamics Study. *J. Chem. Phys.* **2013**, *139*, 114508.
- (17) Yoon, H.; Howlett, P. C.; Best, a. S.; Forsyth, M.; MacFarlane, D. R. Fast Charge/Discharge of Li Metal Batteries Using an Ionic Liquid Electrolyte. *J. Electrochem. Soc.* **2013**, *160*, A1629—A1637.
- (18) Haskins, J. B.; Bennett, W. R.; Wu, J. J.; Hernández, D. M.; Borodin, O.; Monk, J. D.; Bauschlicher, C. W.; Lawson, J. W. Computational and Experimental Investigation of Li-Doped Ionic Liquid Electrolytes: [PYR14][TFSI], [PYR13][FSI], and [EMIM]-[BF4]. J. Phys. Chem. B 2014, 118, 11295–11309.
- (19) Menne, S.; Vogl, T.; Balducci, A. Lithium Coordination in Protic Ionic Liquids. *Phys. Chem. Chem. Phys.* **2014**, *16*, 5485–5489.
- (20) Duluard, S.; Grondin, J.; Bruneel, J.-L.; Pianet, I.; Grelard, A.; Campet, G.; Delville, M.-H.; Lassegues, J.-C. Lithium Solvation and Diffusion in the 1-Butyl-3-Methylimidazolium Bis-(trifluoromethanesulfonyl)imide Ionic Liquid. *J. Raman Spectrosc.* 2008, 39, 627–632.
- (21) Monteiro, M. J.; Bazito, F. F. C.; Siqueira, L. J. A.; Ribeiro, M. C. C.; Torresi, R. M. Transport Coefficients, Raman Spectroscopy, and Computer Simulation of Lithium Salt Solutions in an Ionic Liquid. *J. Phys. Chem. B* **2008**, *112*, 2102–2109.

- (22) Kunze, M.; Jeong, S.; Paillard, E.; Schönhoff, M.; Winter, M.; Passerini, S. New Insights to Self-Aggregation in Ionic Liquid Electrolytes for High-Energy Electrochemical Devices. *Adv. Energy Mater.* **2011**, *1*, 274–281.
- (23) Castriota, M.; Caruso, T.; Agostino, R. G.; Cazzanelli, E.; Henderson, W. A.; Passerini, S. Raman Investigation of the Ionic Liquid N-Methyl-N-Propylpyrrolidinium Bis-(trifluoromethanesulfonyl)imide and Its Mixture with LiN(SO<sub>2</sub>CF<sub>3</sub>)<sub>2</sub>. *J. Phys. Chem. A* **2005**, *109*, 92–96.
- (24) Umebayashi, Y.; Mitsugi, T.; Fukuda, S.; Fujimori, T.; Fujii, K.; Kanzaki, R.; Takeuchi, M.; Ishiguro, S. I. Lithium Ion Solvation in Room-Temperature Ionic Liquids Involving Bis-(trifluoromethanesulfonyl) Imide Anion Studied by Raman Spectroscopy and DFT Calculations. J. Phys. Chem. B 2007, 111, 13028—13032.
- (25) Lassègues, J.-C.; Grondin, J.; Talaga, D. Lithium Solvation in Bis(trifluoromethanesulfonyl)imide-Based Ionic Liquids. *Phys. Chem. Chem. Phys.* **2006**, *8*, 5629–5632.
- (26) Herstedt, M.; Smirnov, M.; Johansson, P.; Chami, M.; Grondin, J.; Servant, L.; Lassegues, J. C. Spectroscopic Characterization of the Conformational States of the Bis (Trifluoromethanesulfonyl) Imide Anion (TFSI). *J. Raman Spectrosc.* **2005**, *36*, 762–770.
- (27) Umebayashi, Y.; Mori, S.; Fujii, K.; Tsuzuki, S.; Seki, S.; Hayamizu, K.; Ishiguro, S. Raman Spectroscopic Studies and Ab Initio Calculations on Conformational Isomerism of 1-Butyl-3-Methylimidazolium Bis-(Trifluoromethanesulfonyl) amide Solvated to a Lithium Ion in Ionic Liquids: Effects of the Second Solvation Sphere of the Lithium Ion. *J. Phys. Chem. B* **2010**, *114*, 6513–6521.
- (28) Shirai, A.; Fujii, K.; Seki, S.; Umebayashi, Y.; Ishiguro, S.-i.; Ikeda, Y. Solvation of Lithium Ion in N,N-Diethyl-N-Methyl-N- (2-Methoxyethyl)ammonium Bis(trifluoromethanesulfonyl)- Amide Using Raman and Multinuclear NMR Spectroscopy. *Anal. Sci.* 2008, 24, 1291–1296.
- (29) Lahiri, A.; Schubert, T. J. S.; Iliev, B.; Endres, F. LiTFSI in 1-Butyl-1-Methylpyrrolidinium Bis(fluorosulfonyl)amide: A Possible Electrolyte for Ionic Liquid Based Lithium Ion Batteries. *Phys. Chem. Chem. Phys.* **2015**, *17*, 11161–11164.
- (30) Huang, J.; Hollenkamp, A. F. Thermal Behavior of Ionic Liquids Containing the FSI Anion and the Li<sup>+</sup> Cation. *J. Phys. Chem.* C **2010**, *114*, 21840–21847.
- (31) Lahiri, A.; Carstens, T.; Atkin, R.; Borisenko, N.; Endres, F. In Situ Atomic Force Microscopic Studies of the Interfacial Multilayer Nanostructure of LiTFSI–[Py<sub>1,4</sub>]TFSI on Au(111): Influence of Li <sup>+</sup> Ion Concentration on the Au(111)/IL Interface. *J. Phys. Chem. C* **2015**, *119*, 16734–16742.
- (32) Umebayashi, Y.; Mitsugi, T.; Fukuda, S.; Fujimori, T.; Fujii, K.; Kanzaki, R.; Takeuchi, M.; Ishiguro, S. Lithium Ion Solvation in Room-Temperature Ionic Liquids Involving Bis (Trifluoromethanesulfonyl) Imide Anion Studied by Raman Spectroscopy and DFT Calculations. *J. Phys. Chem. B* **2007**, *111*, 13028–13032.
- (33) Fujii, K.; Hamano, H.; Doi, H.; Song, X.; Tsuzuki, S.; Hayamizu, K.; Seki, S.; Kameda, Y.; Dokko, K.; Watanabe, M.; et al. Unusual Li<sup>+</sup> Ion Solvation Structure in Bis(Fl Uorosulfonyl)amide Based Ionic Liquid. *J. Phys. Chem. C* **2013**, *117*, 19314–19324.
- (34) Lesch, V.; Jeremias, S.; Moretti, A.; Passerini, S.; Heuer, A.; Borodin, O. A Combined Theoretical and Experimental Study of the Influence of Different Anion Ratios on Lithium Ion Dynamics in Ionic Liquids. *J. Phys. Chem. B* **2014**, *118*, 7367–7375.
- (35) Borodin, O.; Smith, G. D.; Henderson, W. Li<sup>+</sup> Cation Environment, Transport, and Mechanical Properties of the LiTFSI Doped N-Methyl-N-alkylpyrrolidinium<sup>+</sup>TFSI Ionic Liquids. *J. Phys. Chem. B* **2006**, *110*, 16879–16886.
- (36) Tobishima, S.; Arakawa, M.; Hirai, T.; Yamaki, J. Ethylene Carbonate-Based Electrolytes for Rechargeable Lithium Batteries. *J. Power Sources* **1989**, 26, 449–454.
- (37) Guyomard, D.; Tarascon, J. M. Li Metal-Free Rechargeable LiMn<sub>2</sub>O<sub>4</sub>/Carbon Cells: Their Understanding and Optimization. *J. Electrochem. Soc.* **1992**, *139*, 937–948.

- (38) Tarascon, J. M.; Guyomard, D.; Baker, G. L. An Update of the Li Metal-Free Rechargeable Battery Based on Li<sup>1+</sup> $\chi$ Mn<sub>2</sub>O<sub>4</sub> Cathodes and Carbon Anodes. *J. Power Sources* **1993**, *44*, 689–700.
- (39) Ohzuku, T.; Iwakoshi, Y.; Sawai, K. Formation of Lithium-Graphite Intercalation Compounds in Nonaqueous Electrolytes and Their Application as a Negative Electrode for a Lithium Ion (Shuttlecock) Cell. *J. Electrochem. Soc.* 1993, 140, 2490.
- (40) Appetecchi, G. B.; Montanino, M.; Balducci, A.; Lux, S. F.; Winterb, M.; Passerini, S. Lithium Insertion in Graphite Fromternary Ionic Liquid-Lithium Salt Electrolytes I. Electrochemical Characterization of the Electrolytes. *J. Power Sources* **2009**, *192*, 599–605.
- (41) Lux, S. F.; Schmuck, M.; Appetecchi, G. B.; Passerini, S.; Winter, M.; Balducci, A. Lithium Insertion in Graphite Fromternary Ionic Liquid—lithium Salt Electrolytes: II. Evaluation of Specific Capacity and Cycling Efficiency and Stability at Room Temperature. *J. Power Sources* **2009**, *192*, 606—611.
- (42) Moreno, M.; Simonetti, E.; Appetecchi, G. B.; Carewska, M.; Montanino, M.; Kim, G.-T.; Loeffler, N.; Passerini, S. Ionic Liquid Electrolytes for Safer Lithium Batteries. *J. Electrochem. Soc.* **2017**, *164*, A6026—A6031.
- (43) Vogel, H. The Law of Relation between the Viscosity of Liquids and the Temperature. *Phys. Zeitschrift* **1921**, 22, 645–646.
- (44) Fulcher, G. S. Analysis of Recent Measurements of Viscosity of Glasses. J. Am. Ceram. Soc. 1925, 8, 339–355.
- (45) Tammann, G.; Hesse, W. The Dependence of Viscosity upon the Temperature of Supercooled Liquids. Zeitschrift für Anorg. und Allg. Chemie 1926, 156, 245–257.
- (46) Bruce, P. G.; Vincent, C. A. Steady State Current Flow in Solid Binary Electrolyte Cells. *J. Electroanal. Chem. Interfacial Electrochem.* 1987, 225, 1–17.
- (47) Zhang, S.; Sun, N.; He, X.; Lu, X.; Zhang, X. Physical Properties of Ionic Liquids: Database and Evaluation. *J. Phys. Chem. Ref. Data* **2006**, *35*, 1475–1517.
- (48) Furlani, M.; Albinsson, I.; Mellander, B. E.; Appetecchi, G. B.; Passerini, S. Annealing Protocols for Pyrrolidinium Bis-(trifluoromethylsulfonyl)imide Type Ionic Liquids. *Electrochim. Acta* **2011**, *57*, 220–227.
- (49) Carstens, T.; Lahiri, A.; Borisenko, N.; Endres, F. [Py<sub>1,4</sub>]-FSI-NaFSI-Based Ionic Liquid Electrolyte for Sodium Batteries: Na<sub>+</sub> solvation and Interfacial Nanostructure on Au(111). *J. Phys. Chem. C* **2016**, 120, 14736–14741.
- (50) Niu, S.; Cao, Z.; Li, S.; Yan, T. Hexafluorophosphate Ionic Liquids: A Molecular Dynamics Study. *J. Phys. Chem. B* **2010**, *114*, 877–881.
- (51) Yamada, A.; Chung, S. C.; Hinokuma, K. Optimized LiFePO<sub>4</sub> for Lithium Battery Cathodes. *J. Electrochem. Soc.* **2001**, *148*, A224.
- (52) Sinha, N. N.; Burns, J. C.; Sanderson, R. J.; Dahn, J. Comparative Studies of Hardware Corrosion at High Potentials in Coin-Type Cells with Non Aqueous Electrolytes. *J. Electrochem. Soc.* **2011**, *158*, A1400—A1403.
- (53) Kasnatscheew, J.; Cao, X.; Röser, S.; Janßen, P.; Winter, M.; Cekic-Laskovic, I.; Streipert, B.; Wagner, R. Influence of LiPF<sub>6</sub> on the Aluminum Current Collector Dissolution in High Voltage Lithium Ion Batteries after Long-Term Charge/Discharge Experiments. *J. Electrochem. Soc.* **2017**, *164*, A1474—A1479.
- (54) Pyschik, M.; Kraft, V.; Passerini, S.; Winter, M.; Nowak, S. Thermal Aging of Anions in Ionic Liquids Containing Lithium Salts by IC/ESI-MS. *Electrochim. Acta* **2014**, *130*, 426–430.

# Pyrrolidinium Ionic Liquid Electrolyte with Bis(trifluoromethylsulfonyl)imide and Bis(fluorosulfonyl)imide Anions: Lithium Solvation and Mobility, and Performance in Lithium Metal—Lithium Iron Phosphate Batteries

# **Supporting information**

Qianwen Huang<sup>†</sup>, Yun-Yang Lee<sup>†</sup>, Burcu Gurkan<sup>\*</sup>

Department of Chemical and Biomolecular Engineering, Case Western Reserve University, Cleveland, OH 44106, USA

\* Corresponding author: beg23@case.edu

† Authors contributed equally

**Table S1.** Measured water contents of the studied samples before physical property measurements.

l	
IL	Water content
	(ppm)
[PYR13][TFSI]	76
[PYR13][FSI]	127
[PYR13][TFSI]/[PYR13][FSI] (v:v = 1:9)	231
[PYR13][TFSI]/[PYR13][FSI] (v:v = 1:1)	158
[PYR13][TFSI]/[PYR13][FSI] (v:v = 9:1)	157
0.1 M LiFSI in [PYR13][FSI]	746
0.2 M LiFSI in [PYR13][FSI]	117
0.5 M LiFSI in [PYR13][FSI]	223
1 M LiFSI in [PYR13][FSI]	114
0.1 M LiFSI in [PYR13][TFSI]	378
0.2 M LiFSI in [PYR13][TFSI]	564
0.5 M LiFSI in [PYR13][TFSI]	452
1 M LiFSI in [PYR13][TFSI]	657
0.1 M LiFSI in [PYR13][TFSI]/[PYR13][FSI] (v:v = 1:1)	349
0.2 M LiFSI in [PYR13][TFSI]/[PYR13][FSI] (v:v = 1:1)	314
0.5 M LiFSI in [PYR13][TFSI]/[PYR13][FSI] (v:v = 1:1)	660
1 M LiFSI in [PYR13][TFSI]/[PYR13][FSI] (v:v = 1:1)	206

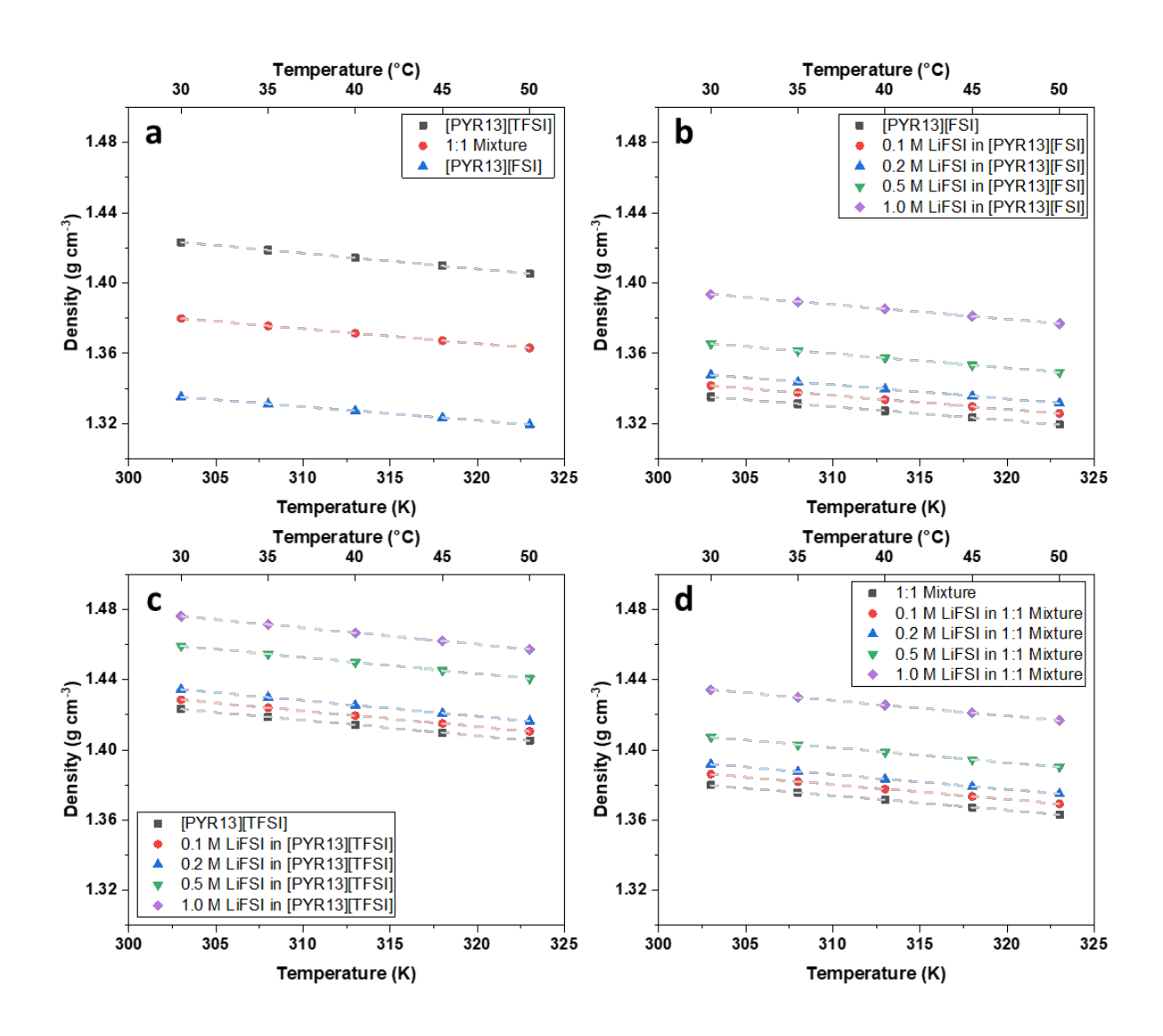


**Figure S1**. Density of [PYR13][TFSI]/[PYR13][FSI] (a), LiFSI/[PYR13][FSI] (b), LiFSI/[PYR13][TFSI] (c) and LiFSI/[PYR13][TFSI]/[PYR13][FSI] (1:1, v/v) (d). The dashed lines are linear fits.

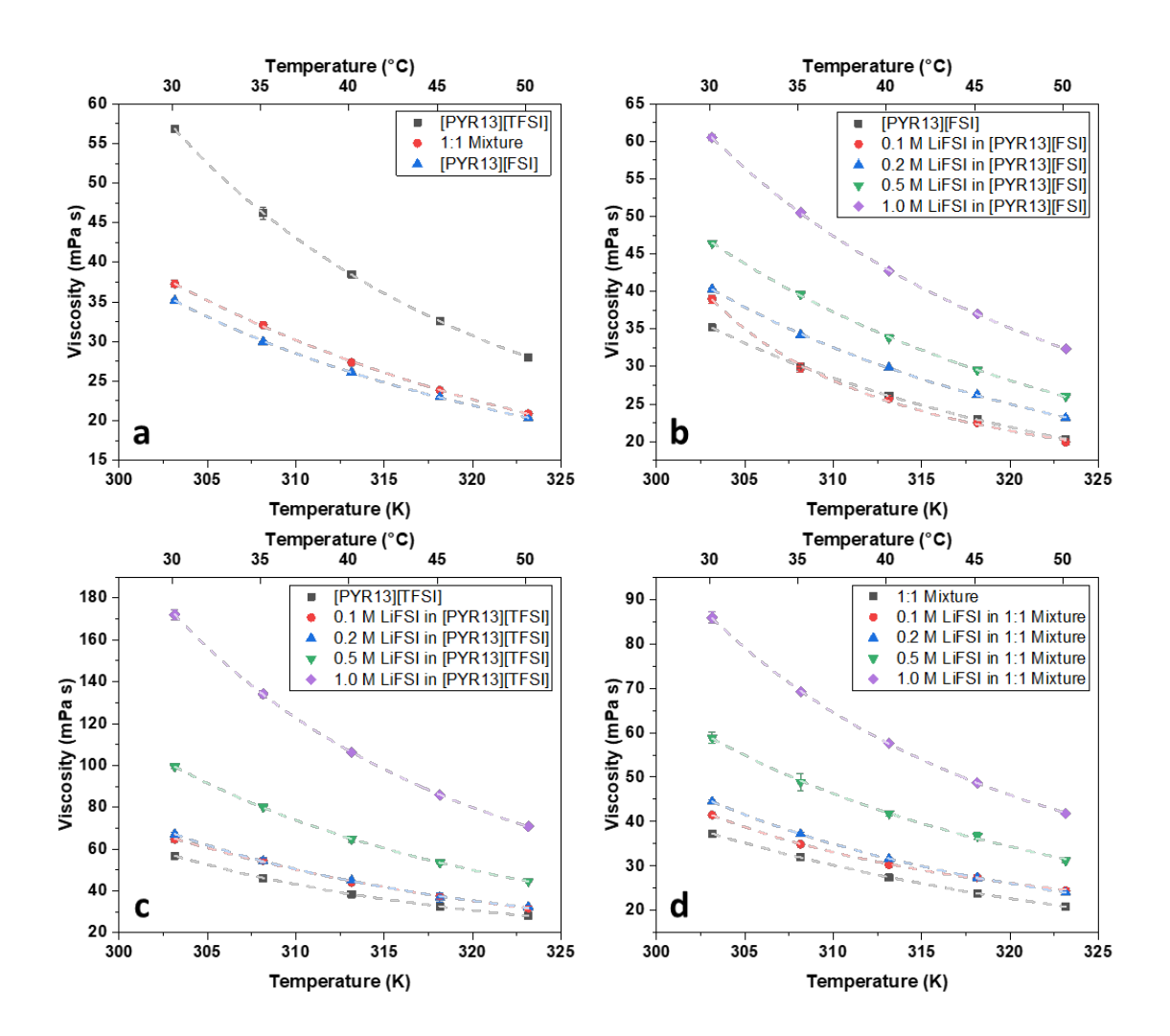


Figure S2. Viscosity of [PYR13][TFSI]/[PYR13][FSI] (a), [Li][FSI]/[PYR13][FSI] (b), [Li][FSI]/[PYR13][TFSI] (c) and [Li][FSI]/[PYR13][TFSI]/[PYR13][FSI] (1:1, v/v) (d). The dashed lines are the VFT fits that express viscosity as  $\mu=\mu_0exp(\frac{E_a}{T-T_0})$ .

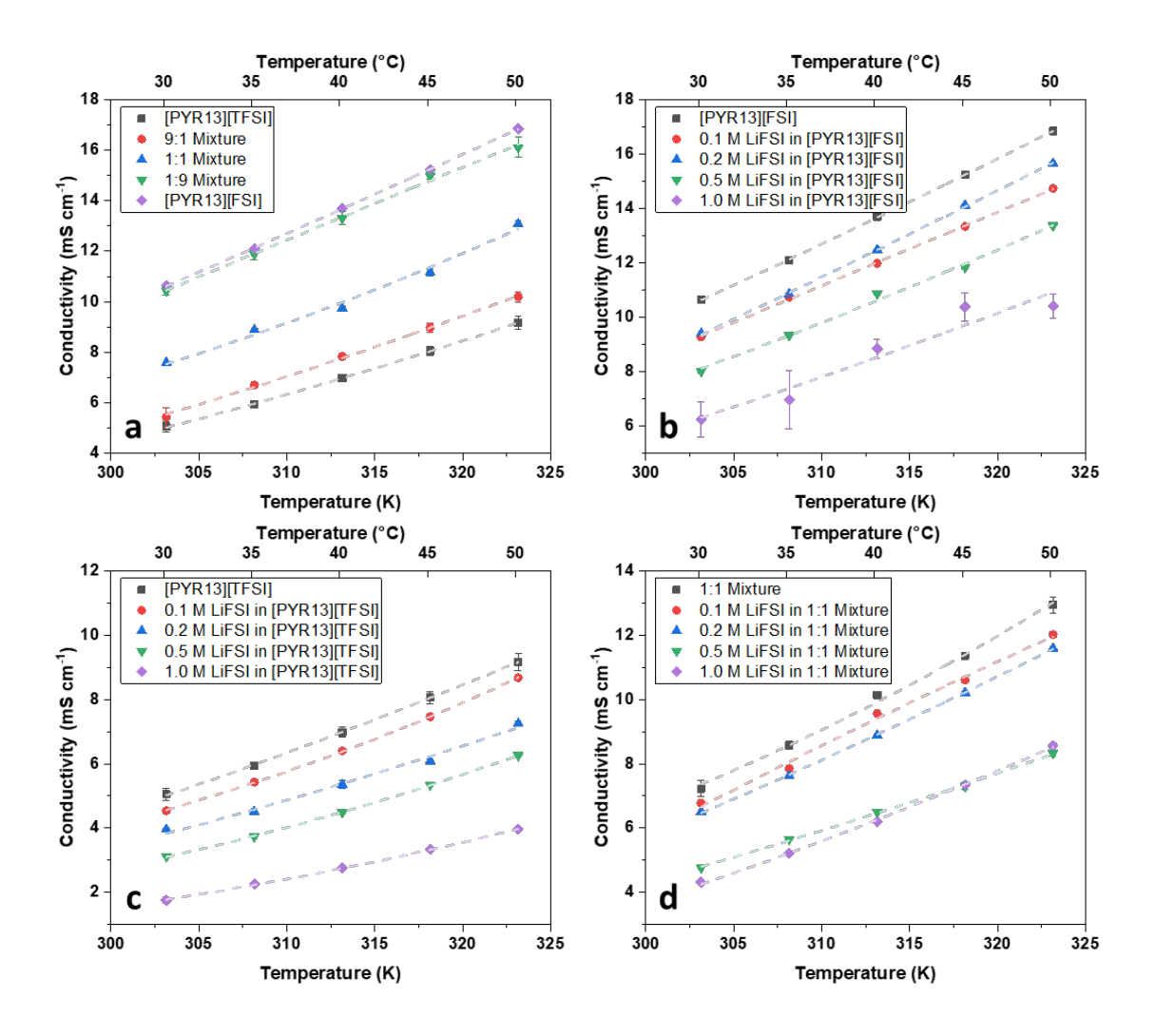


Figure S3. Conductivity of [PYR13][TFSI]/[PYR13][FSI] (a), [Li][FSI]/[PYR13][FSI] (b), [Li][FSI]/[PYR13][TFSI]/[PYR13][FSI]/[PYR13][FSI] (1:1, v/v) (d). The dashed lines are the modified-VFT fits that express ionic conductivity as  $\sigma = \sigma_0 T^{1/2} exp(\frac{E_a'}{T-T_0}).$ 

**Table S2**. Vogel-Fulcher-Tamman (VFT) parameters of conductivity and viscosity for IL/IL, [Li][FSI]/IL, and [Li][FSI]/IL/IL mixtures.

IL	Т	μ	μ =	$\mu = \mu_0 exp(\frac{E_a}{T - T_0})$		σ	$\sigma = \sigma_0 T^{1/2} exp(\frac{E_a'}{T - T_0})$			ρ	$ \rho \\ = A + B \\ \times 10^{-3} T $	
	(K)	(cP)	$\mu_0$	$E_a$	$T_0$	(mS/cm)	$\sigma_0$	$E_a'$	$T_0$	(g/cm³)	Α	В
	303	56.84				5.05				1.42		
	308	46.19				5.94				1.42		
[PYR13][TFSI]	313	38.48	1.39	314.65	218.30	6.98	5.72	-253.57	218.30	1.41	1.70	-8.97
	318	32.56				8.05				1.41		
	323	28.00				9.17				1.41		
	303	37.25				7.23				1.38		
	308	32.08				8.57				1.38		
[PYR13][TFSI]/[PYR13][FSI] (v:v = 1:1)	313	27.37	0.06	1277.21	103.36	10.14	155.32	- 1180.02	103.36	1.37	1.63	-8.38
( =:=/	318	23.84				11.36				1.37		
	323	20.90				12.94				1.36		
	303	35.19				10.64				1.34		
	308	29.98				12.10				1.33		
[PYR13][FSI]	313	26.13	1.50	301.98	207.47	13.69	7.26	-236.78	207.47	1.33	1.43	-2.82
	318	22.98				15.23				1.32		
	323	20.33				16.84				1.32		
		<b>r</b>	ı	r	<b>r</b>		r	1	r	r	1	
	303	35.19				10.64				1.34		
	308	29.98				12.10				1.33		
[PYR13][FSI]	313	26.13	1.50	301.98	207.47	13.69	7.26	-236.78	207.47	1.33	1.43	-0.28
	318	22.98				15.23				1.32		
	323	20.33				16.84				1.32		
	303	39.01				9.28				1.34		
	308	29.85				10.74				1.34		
0.1 M [Li][FSI] in [PYR13][FSI]	313	25.71	9.65	31.43	280.63	11.98	24.45	-22.40	280.63	1.33	1.58	0.79
	318	22.50				13.33				1.33		
	323	19.92				14.73				1.33		
	303	40.32				9.40				1.35		
	308	34.23				10.85				1.34		
0.2 M [Li][FSI] in [PYR13][FSI]	313	29.85	1.81	288.21	210.32	12.48	169.54	-268.52	210.32	1.34	1.59	-0.80
	318	26.25				14.11				1.34		
	323	23.15				15.65				1.33		
	303	46.44	0.87	462.84	186.66	8.02	11.30	-371.27	186.66	1.37	1.61	-0.81

1	308	39.62				9.33				1.36		
0.5 M [Li][FSI] in [PYR13][FSI]	313	33.82				10.86				1.36		
	318	29.53				11.84				1.35		
	323	26.01				13.36				1.35		
	303	60.52				6.26				1.39		
	308	50.53				6.97				1.39		
1 M [Li][FSI] in [PYR13][FSI]	313	42.77	2.13	290.75	216.28	8.84	5.74	-239.90	216.28	1.39	1.64	-0.83
[i iiii]	318	37.00				10.38				1.38		
	323	32.37				10.41				1.38		
		u e	ı	l.		l .	l.	l.				
	303	56.84				5.05				1.42		
	308	46.19				5.94				1.42		
[PYR13][TFSI]	313	38.48	1.39	314.65	218.30	6.98	5.72	-253.57	218.30	1.41	1.70	-0.90
	318	32.56				8.05				1.41		
	323	28.00				9.17				1.41		
	303	64.73				4.54				1.43		
	308	54.51				5.43				1.42		
0.1 M [Li][FSI] in [PYR13][TFSI]	313	44.05	0.01	2051.38	74.38	6.40	519.11	- 1736.47	74.38	1.42	1.70	-0.90
[11/123][1131]	318	37.44				7.46				1.41		
	323	31.71				8.67				1.41		
	303	67.12				3.96				1.43		
	308	54.31				4.51				1.43		
0.2 M [Li][FSI] in [PYR13][TFSI]	313	45.01	1.12	370.12	212.73	5.36	5.65	-293.41	212.73	1.43	1.71	0.90
[11123][1131]	318	36.79				6.08				1.42		
	323	32.39				7.25				1.42		
	303	99.34				3.12				1.46		
	308	80.07				3.74				1.45		
0.5 M [Li][FSI] in [PYR13][TFSI]	313	64.64	0.11	1011.22	154.06	4.49	51.69	-845.41	154.06	1.45	1.74	-0.93
[[11123][1131]	318	53.46				5.35				1.45		
	323	44.66				6.26				1.44		
	303	172.07				1.76				1.48		
	308	134.13				2.26				1.47		
1 M [Li][FSI] in [PYR13][TFSI]	313	106.13	0.52	640.53	192.75	2.76	15.17	-551.49	192.75	1.47	1.76	-0.94
[[1][1][1]	318	85.87				3.34				1.46		
	323	70.84				3.96				1.46		
	303	37.25				7.23				1.38		
[PYR13][TFSI]/[PYR13][FSI] (v:v = 1:1)	308	32.08	0.06	1277 21	102.20	8.57	155.32	- 1180.02	103.36	1.38	1.62	-0.84
	313	27.37	0.06	1277.21	103.36	10.14				1.37	1.63	
	318	23.84				11.36				1.37		

	323	20.90				12.94				1.36		
0.1 M [Li][FSI] in [PYR13][TFSI]/[PYR13][FSI]	303	41.48		71.58	259.74	6.78		-75.96	259.74	1.39	1.64	
	308	34.91				7.85				1.38		-0.84
	313	30.33	7.97			9.56	2.20			1.38		
(v:v = 1:1)	318	27.44				10.60				1.37		
	323	24.48				12.01				1.37		
	303	44.50				6.51		-241.05	218.93	1.39	1.65	
0.2 M [Li][FSI] in	308	37.21		270.42	218.93	7.63	6.50			1.39		-0.85
[PYR13][TFSI]/[PYR13][FSI]	313	31.62	1.79			8.89				1.38		
(v:v = 1:1)	318	27.40				10.21				1.38		
	323	24.04				11.59				1.37		
	303	58.84		383.82	201.42	4.77	6.35	-318.93	201.42	1.41	1.67	-0.86
0.5 M [Li][FSI] in	308	48.89				5.66				1.40		
[PYR13][TFSI]/[PYR13][FSI]	313	41.85	1.35			6.50				1.40		
(v:v = 1:1)	318	36.74				7.30				1.39		
	323	31.24				8.33				1.39		
	303	85.87			227.48	4.32		-239.24	227.48	1.43		-0.88
1 M [Li][FSI] in [PYR13][TFSI]/[PYR13][FSI] (v:v = 1:1)	308	69.21		259.42		5.21	5.78			1.43	1.70	
	313	57.68	2.78			6.20				1.43		
	318	48.71				7.34				1.42		
	323	41.84				8.56				1.42		

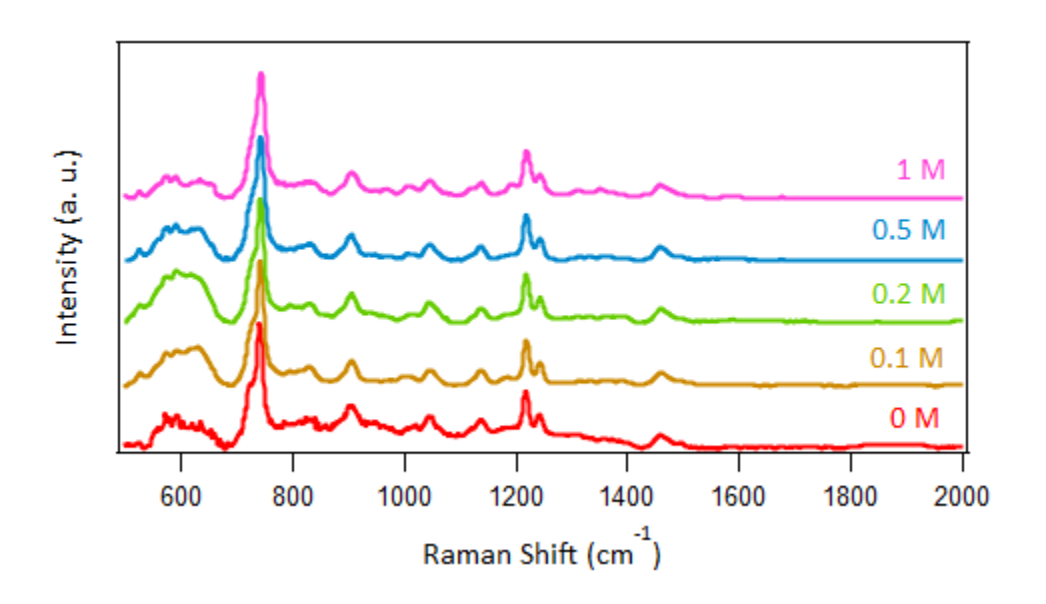


**Figure S4.** Raman spectrum of [Li][FSI] in [PYR13][TFSI]/[PYR13][FSI] (1:1, v/v). The spectral resolution is 6.5 cm<sup>-1</sup>.

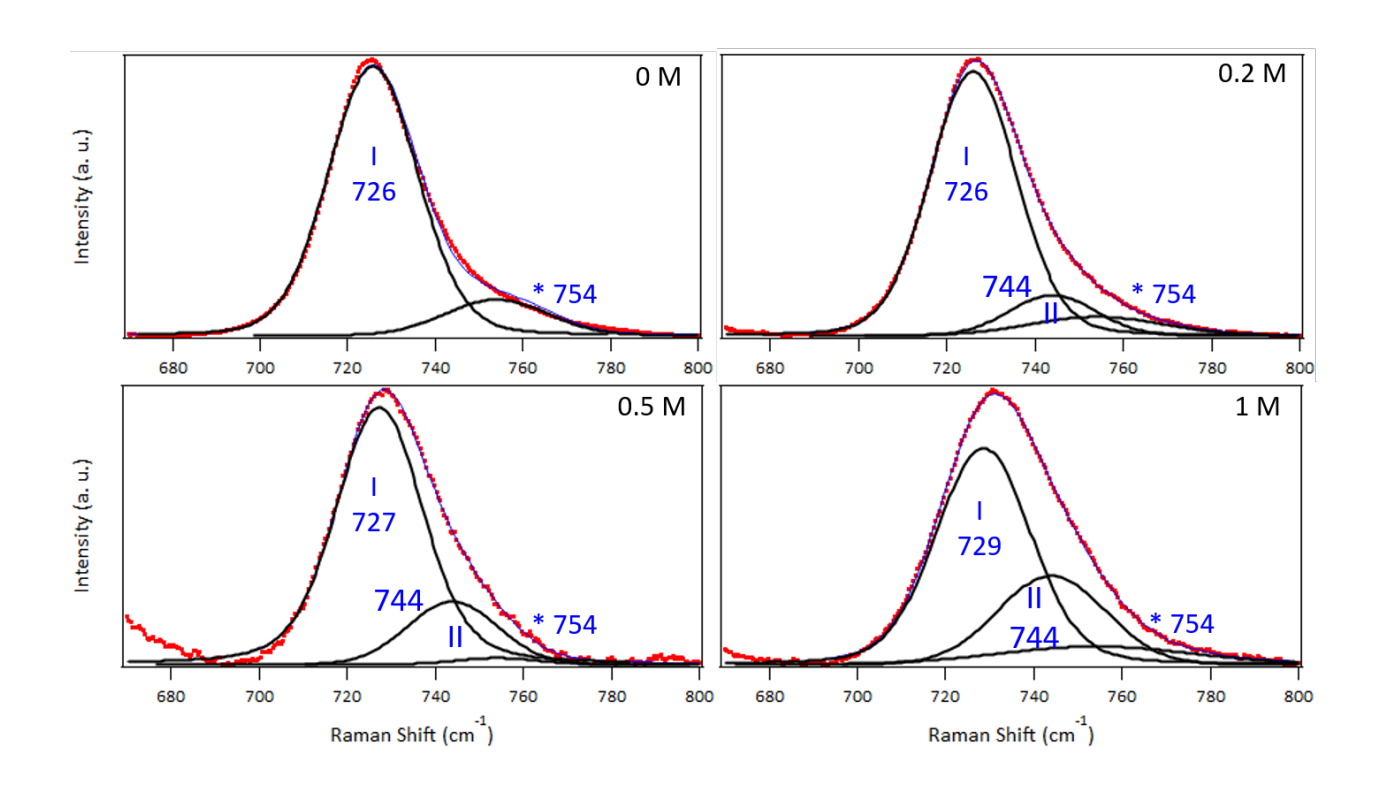
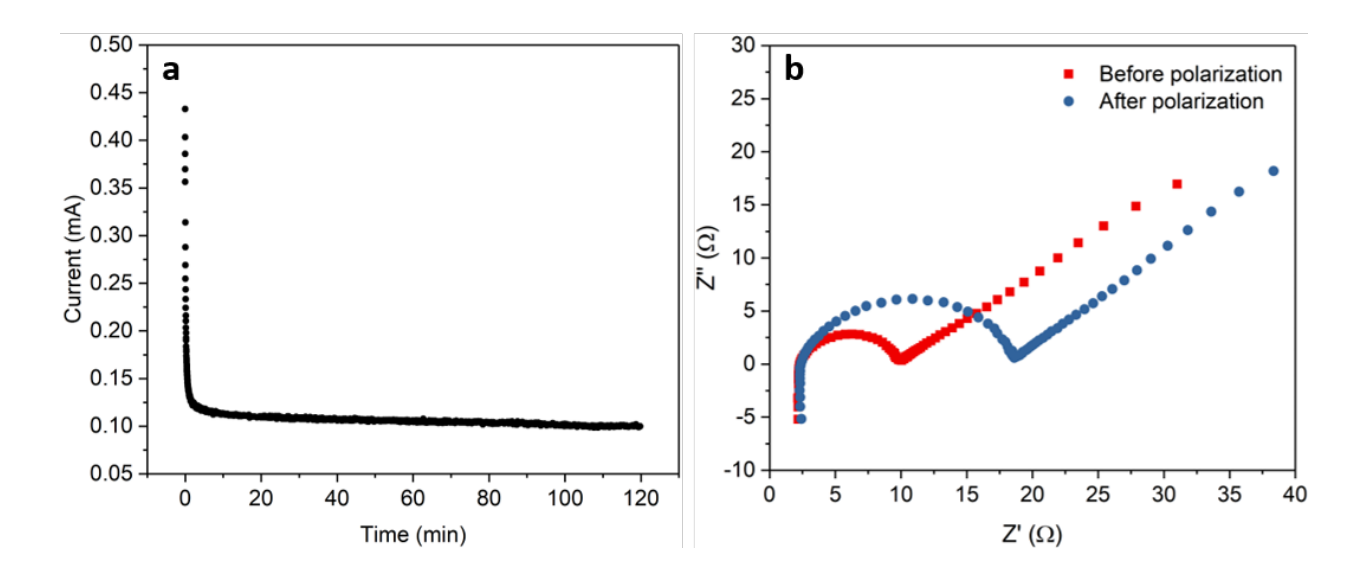
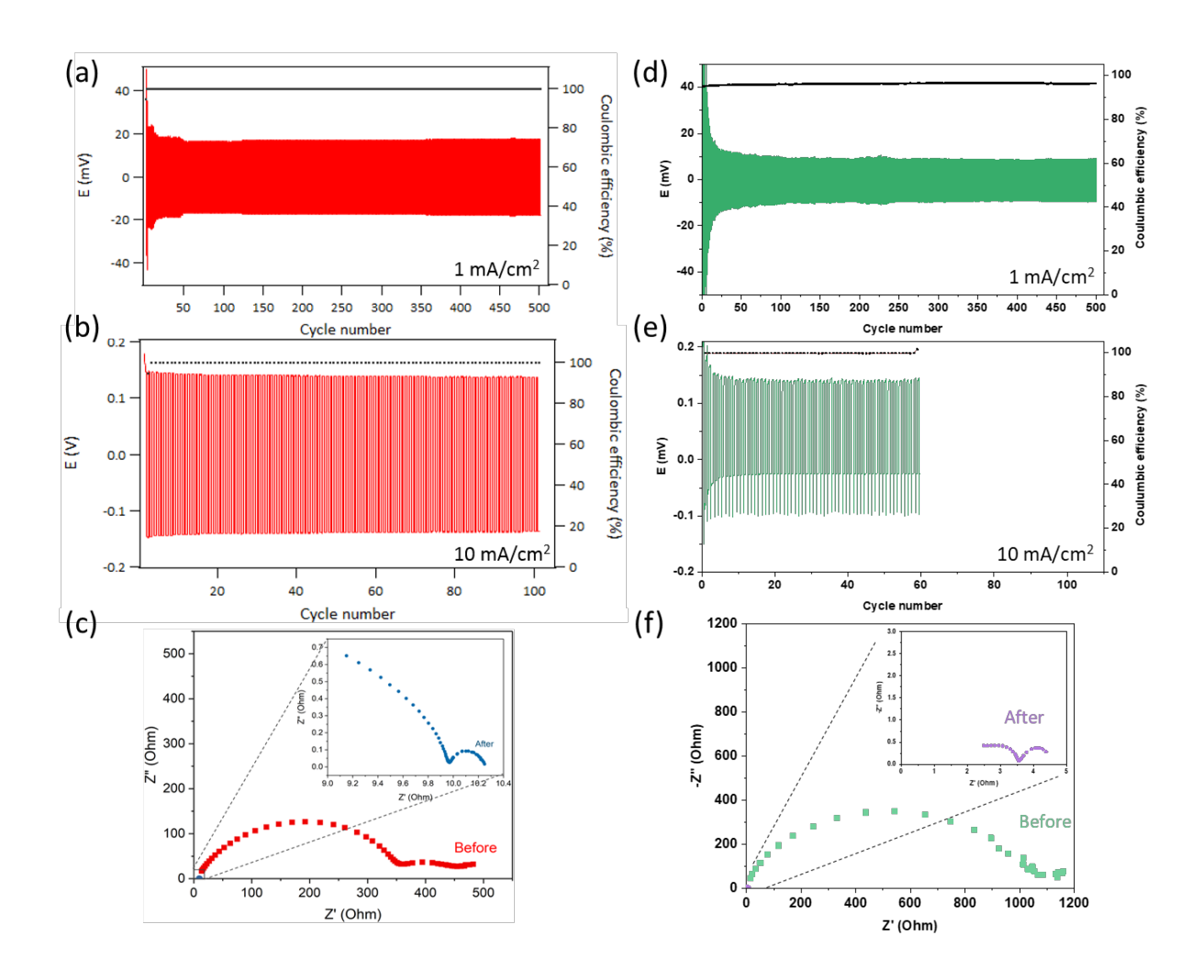


Figure S5. Local Raman spectrum of [Li][FSI]/[PYR13][FSI].



**Figure S6**. (a) The time dependent dc polarization and (b) electrochemical impedance spectroscopy (EIS) of 0.5 M [Li][FSI] in [PYR13][TFSI]/[PYR13][FSI] (1:1, v/v). The DC constant potential applied was 10 mV. The frequency range of the EIS was  $10^{-2}$  to  $10^6$  Hz.



**Figure S7.** Cycling of Li-Li cells with 0.5 M [Li][FSI] in [PYR13][TFSI]/[PYR13][FSI] (1:1, v/v) electrolyte at 20°C. Left panel: cells with glass fiber separator. Right panel: cells with Solupor separator. (a and d) 1 mA/cm<sup>2</sup>, (b and e) 10 mA/cm<sup>2</sup> (c and f) EIS plots before and after 500 cycles at 1 mA/cm<sup>2</sup>.